

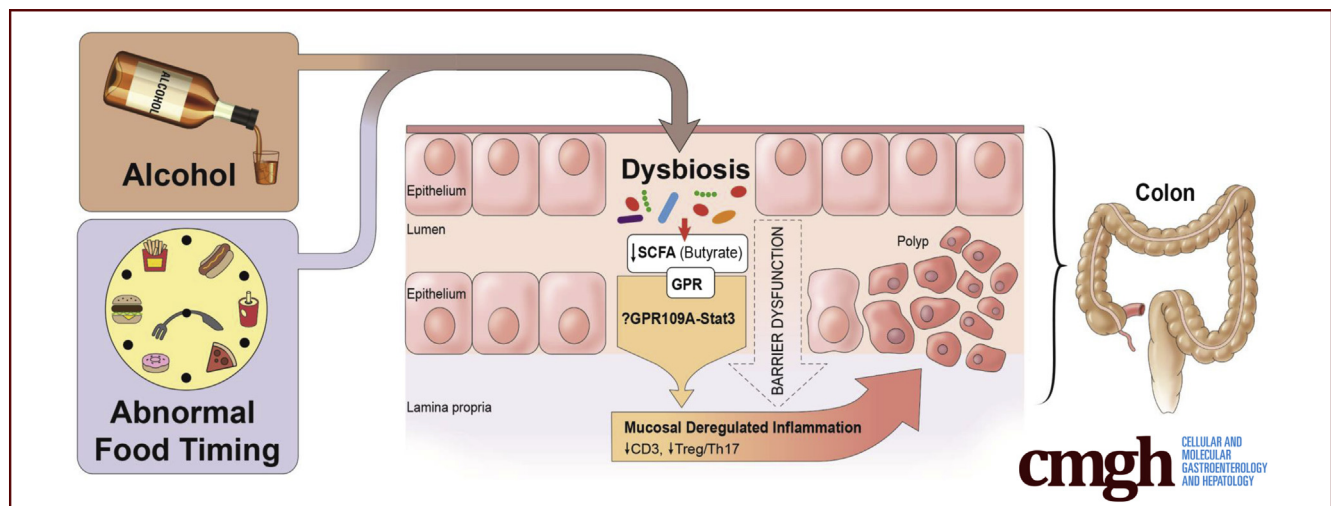
## ORIGINAL RESEARCH

## Abnormal Eating Patterns Cause Circadian Disruption and Promote Alcohol-Associated Colon Carcinogenesis



Faraz Bishehsari,<sup>1</sup> Phillip A. Engen,<sup>1</sup> Robin M. Voigt,<sup>1</sup> Garth Swanson,<sup>1</sup> Maliha Shaikh,<sup>1</sup> Sherry Wilber,<sup>1</sup> Ankur Naqib,<sup>1,2</sup> Stefan J. Green,<sup>2,3</sup> Brandon Shetuni,<sup>4</sup> Christopher B. Forsyth,<sup>1</sup> Abdulrahman Saadalla,<sup>5</sup> Abu Osman,<sup>5</sup> Bruce R. Hamaker,<sup>6</sup> Ali Keshavarzian,<sup>1,7,8</sup> and Khashayarsha Khazaie<sup>5</sup>

<sup>1</sup>Department of Internal Medicine, Division of Gastroenterology, <sup>7</sup>Department of Physiology, Rush University Medical Center, Chicago, Illinois; <sup>2</sup>Sequencing Core, Research Resources Center, <sup>3</sup>Department of Biological Sciences, University of Illinois at Chicago, Chicago, Illinois; <sup>4</sup>Northwestern Medicine, Central DuPage Hospital, Winfield, Illinois; <sup>5</sup>Department of Immunology, Mayo Clinic, Rochester, Minnesota; <sup>6</sup>Whistler Center for Carbohydrate Research, Department of Food Science, Purdue University, West Lafayette, Indiana; <sup>8</sup>Division of Pharmacology, Utrecht Institute for Pharmaceutical Sciences, Utrecht University, Utrecht, The Netherlands



## SUMMARY

Abnormal eating patterns as characterized by eating during a rest period causes circadian rhythm disruption in mice. In the mouse polyposis model, eating during rest exacerbates alcohol-associated colon tumor formation by altering intestinal microbiota and causing a protumorigenic mucosal inflammation.

**BACKGROUND & AIMS:** Alcohol intake with circadian rhythm disruption (CRD) increases colon cancer risk. We hypothesized that eating during or around physiologic rest time, a common habit in modern society, causes CRD and investigated the mechanisms by which it promotes alcohol-associated colon carcinogenesis.

**METHODS:** The effect of feeding time on CRD was assessed using B6 mice expressing a fusion protein of PERIOD2 and LUCIFERASE (PER2::LUC) were used to model colon polyposis and to assess the effects of feeding schedules, alcohol consumption, and prebiotic treatment on microbiota composition,

short-chain fatty acid levels, colon inflammation, and cancer risk. The relationship between butyrate signaling and a proinflammatory profile was assessed by inactivating the butyrate receptor GPR109A.

**RESULTS:** Eating at rest (wrong-time eating [WTE]) shifted the phase of the colon rhythm in PER2::LUC mice. In TS4Cre × APC<sup>lox468</sup> mice, a combination of WTE and alcohol exposure (WTE + alcohol) decreased the levels of short-chain fatty acid-producing bacteria and of butyrate, reduced colonic densities of regulatory T cells, induced a proinflammatory profile characterized by hyperpermeability and an increased mucosal T-helper cell 17/regulatory T cell ratio, and promoted colorectal cancer. Prebiotic treatment improved the mucosal inflammatory profile and attenuated inflammation and cancer. WTE + alcohol-induced polyposis was associated with increased signal transducer and activator of transcription 3 expression. Decreased butyrate signaling activated the epithelial signal transducer and activator of transcription 3 in vitro. The relationship between butyrate signaling and a proinflammatory profile was confirmed in human colorectal cancers using The Cancer Genome Atlas.

**CONCLUSIONS:** Abnormal timing of food intake caused CRD and interacts with alcohol consumption to promote colon carcinogenesis by inducing a protumorigenic inflammatory profile driven by changes in the colon microbiota and butyrate signaling. Accession number of repository for microbiota sequence data: raw FASTQ data were deposited in the NCBI Sequence Read Archive under project PRJNA523141. (*Cell Mol Gastroenterol Hepatol* 2020;9:219–237; <https://doi.org/10.1016/j.jcmgh.2019.10.011>)

**Keywords:** Colon Cancer; Circadian; Alcohol; Food Time; Microbiota; Butyrate.

Colorectal cancer (CRC) is the third most common cancer in the world. Modern-lifestyle-specific factors increase the risk of CRC, as evidenced by dramatic differences in CRC rates between developed and developing nations, increasing CRC rates in populations with recent economic growth who have adopted a modern lifestyle, and the ongoing increase in early onset CRC correlating with lifestyle transitions in younger populations in our 24-hour/7-days-a-week society.<sup>1,2</sup> Even limited alcohol consumption increases the risk of colonic premalignant lesions (polyps) and CRC.<sup>3,4</sup> Nonetheless, only a subset of alcohol consumers develops CRC. The presence of multiple risk factors has been shown to increase CRC risk drastically.<sup>5</sup> Thus, additional factors may promote CRC-related mechanisms in the context of alcohol intake.<sup>5</sup> Our group and others have shown that one such mechanism promoted by alcohol use is the alteration of the intestinal microbiota.<sup>6,7</sup> Therefore, lifestyle factors potentially impact CRC risk by altering the intestinal microbiota and causing fluctuations in intestinal inflammation and tissue microenvironment.<sup>8–12</sup>

We previously identified circadian rhythm disruption (CRD), another hallmark of the modern lifestyle and of chronic disease pathogenesis, as an additional factor modulating alcohol-dependent intestinal damage.<sup>13,14</sup> CRD promotes inflammation-mediated diseases,<sup>15</sup> including CRC,<sup>16</sup> with our data indicating a role for light/dark shifting in promoting alcohol-induced CRC.<sup>17</sup>

Although the central circadian clock in the suprachiasmatic nucleus is regulated by the light/dark cycle, circadian rhythms in peripheral tissues, including those in the gastrointestinal tract, can be entrained by external factors independently of the central clock.<sup>18,19</sup> Time-restricted feeding during rest time can shift circadian oscillation of the peripheral clocks in the liver and colon independently of light effects.<sup>18,19</sup> Therefore, abnormal eating patterns can cause CRD through central and peripheral circadian misalignment without disrupting central rhythms. Abnormal eating patterns, characterized by eating late at night or eating large meals close to the biological rest time, are very common in modern society.<sup>20–23</sup> We hypothesize that such patterns cause a central-intestinal CRD that alters the microbiome and enhances alcohol-induced intestinal inflammation and colon carcinogenesis.

## Results

### *Eating During Rest Time Induces Intestinal CRD and Promotes Alcohol-Induced Polyposis*


We first investigated whether rest time eating (wrong-time eating [WTE]) causes CRD in mice. B6 PER2:LUC mice were fed a regular chow diet during light/rest or dark/active phases for 7 days (Figure 1A). WTE for 7 days significantly shifted the acrophase (time of peak expression) (Figure 1B), as well as the circadian rhythm-adjusted mean (Figure 1C) of the colonic rhythm, as measured via the *Per2* promoter activity. The central circadian rhythm was not affected significantly by WTE (Figure 1D). Therefore, WTE disrupts circadian rhythms by causing peripheral-central circadian dyssynchrony.

To model CRC, we used TS4Cre × APC<sup>Δ468</sup> (TS4/APC) mice, with disruption of the adenomatous polyposis coli gene and increased polyposis in the colon and distal ileum.<sup>24</sup> Mice were exposed to WTE or right-time eating (RTE) regimens, either alcohol-treated (RTE + alcohol or WTE + alcohol) or water-treated (RTE + water, WTE + water, and water ad libitum) (Figure 2A). Feeding time did not affect weight or alcohol intake (Figure 2B). No differences in polyp numbers were observed among the water-treated groups, suggesting that the feeding protocol did not impact polyp numbers of water-treated animals (Figure 2C). Compared with water-treated animals, WTE + alcohol mice had a higher tumor burden with more polyps in general, and a higher number of large polyps in particular (Figure 2D). Histologically, lesions in the WTE + alcohol group were more advanced: tumors frequently showed features of high-grade dysplasia/carcinoma in situ, with stratified prominent nuclei, back-to-back glands, and cribriforming gland formation (Figure 2E). These results indicate that CRD caused by WTE predisposes CRC-susceptible mice to alcohol-induced colon cancer.

### *Accelerated Polyposis Correlates With Intestinal Dysbiosis*

Intestinal microbiota can mediate susceptibility to environment-induced colon inflammation and cancer. We have shown that alcohol and CRD can interact to promote dysbiosis.<sup>13</sup> Thus, we next tested whether the exacerbation of polyposis in WTE + alcohol mice is associated with gut microbial dysbiosis when compared with the RTE + alcohol and RTE + water-treated group (hereinafter referred to as

**Abbreviations used in this paper:** ANOSIM, analysis of similarity; ANOVA, analysis of variance; CCL, Chemokine ligand; CRC, colorectal cancer; CRD, circadian rhythm disruption; eTreg, extrathymically induced FOXP3<sup>+</sup> regulatory T cell; GPR, G-protein-coupled receptor; ROR $\gamma$ t<sup>+</sup>, RAR-related orphan receptor  $\gamma$ -positive; RTE, right-time eating; eating during active phase; SCFA, short-chain fatty acid; STAT3, signal transducer and activator of transcription 3; Th, T-helper; Treg, regulatory T cell; TS4/APC, TS4Cre × APC<sup>Δ468</sup>; WTE, wrong-time eating; eating during rest phase; ZT, Zeitgeber time.

 Most current article

© 2020 The Authors. Published by Elsevier Inc. on behalf of the AGA Institute. This is an open access article under the CC BY-NC-ND license (<http://creativecommons.org/licenses/by-nc-nd/4.0/>).

2352-345X

<https://doi.org/10.1016/j.jcmgh.2019.10.011>

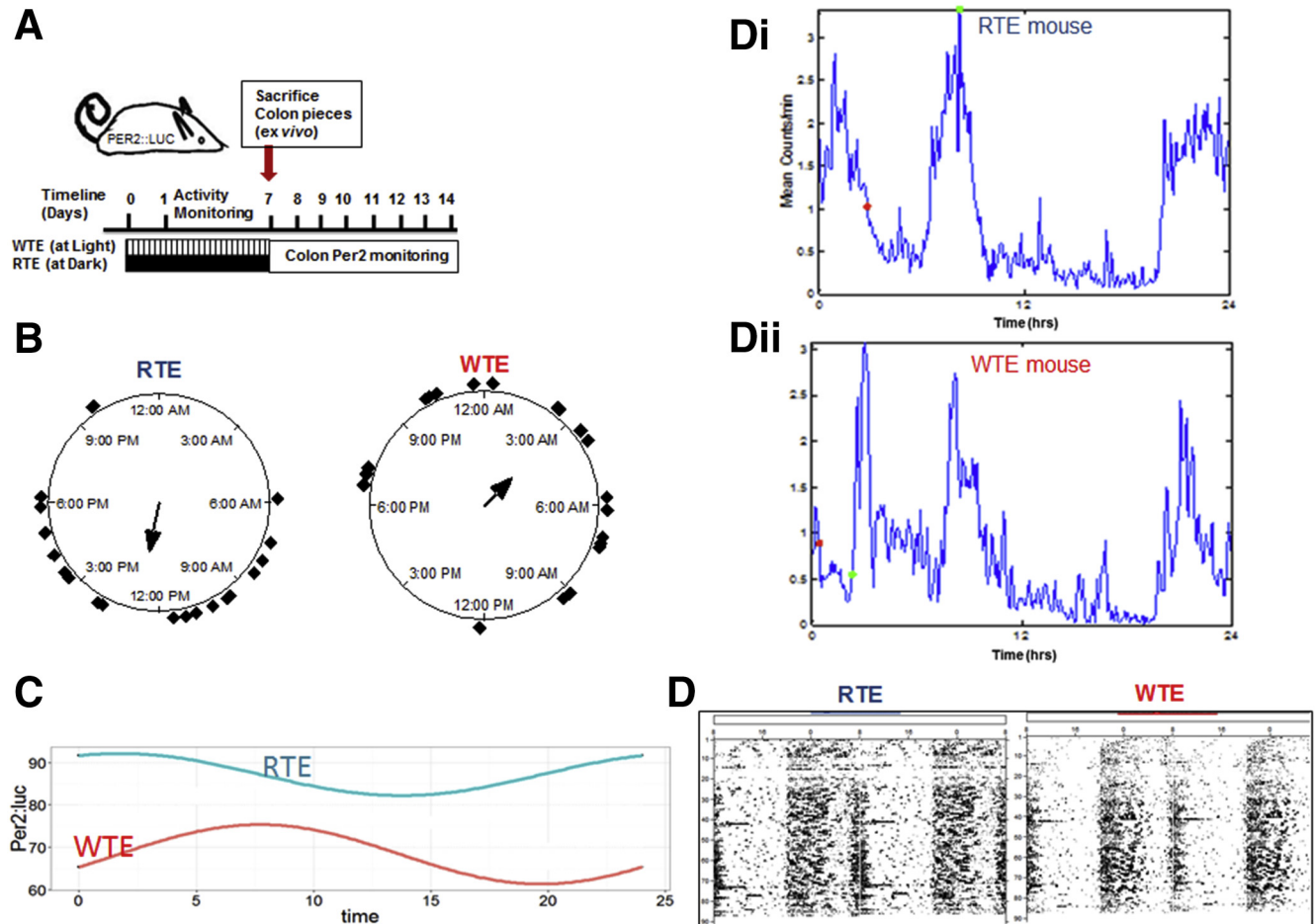


**Figure 1. Rest/wrong-time eating causes circadian rhythm disruption.** (A) B6 PER2::LUC mice ( $n = 5/\text{group}$ ) were fed chow and water during active (at dark: right time) or rest (at light: wrong time) periods for 7 days. Infrared sensors were used to monitor locomotor activity circadian rhythms, with counts collected every 5 minutes. After killing, 3 colon sections per mouse were monitored for bioluminescence activity in 4-hour intervals for 7 days to assess *Per2* expression. (B) WTE vs RTE shifted the phase ( $P < .01$ ) as well as (C) changed the circadian rhythm-adjusted mean of the colonic rhythm ( $P < .01$ ). (D) Average actograms of RTE (left) and WTE (right) mice, showing nocturnal activity and a 2- to 3-hour bout of activity after ZT0. Average waveforms for each group were calculated using individual waveforms of relative activity. Representative activity of 1 mouse per RTE and WTE group is shown in panel Di and Dii, respectively. Time is expressed on the x-axis, with 12 defined as the time of lights off in the light/dark cycle.

control water/H<sub>2</sub>O) fecal samples. Alpha diversity measures, including the Shannon Index (1-way analysis of variance [ANOVA]:  $F_{(2, 12)} = 6.279$ ;  $P = .014$ ) and evenness (1-way ANOVA: (treatment)  $F_{(2, 12)} = 11.20$ ;  $P = .002$ ) were significantly lower in WTE + alcohol treatment relative to other treatments (Figure 3A). Richness and Simpson's index were not significantly different between groups (data not shown).

The structure of fecal microbial communities was significantly different between the treatment groups (analysis of similarity [ANOSIM]: global  $R = 0.232$ ; global  $P = .025$ ) (control water vs WTE + alcohol:  $R = 0.27$ ,  $P = .056$ ; RTE + alcohol vs WTE + alcohol:  $R = 0.45$ ,  $P = .016$ ; control water vs RTE + alcohol:  $R = -0.11$ ,  $P = .74$ ).

Alcohol and CRD reduce the abundance of intestinal short-chain fatty acid (SCFA)-producing bacteria in wild-type mice.<sup>13</sup> Intestinal microbiota impact colon

carcinogenesis, in part via modulating SCFA levels, in particular that of butyrate.<sup>25,26</sup> The effects of treatment on individual fecal microbial taxa (taxonomic levels of family and genus) are shown in Figure 3B. When compared with both control water and RTE + alcohol, the WTE + alcohol fecal samples ( $P < .05$ ) had a higher relative abundance of bacteria from the tumor-associated bacterial family Turcibacteraceae and genus *Turcibacter* and a lower relative abundance of putative SCFA-producing bacteria from the family Lachnospiraceae. No trending or significant differences in the relative abundance of taxa were observed between control water and RTE + alcohol treatments.

The similarity of samples within treatment groups and between treatment groups was assessed using the Bray-Curtis similarity index at the taxonomic level of genus. Analysis of within-group Bray-Curtis similarity showed greater within-treatment variability between animals in the

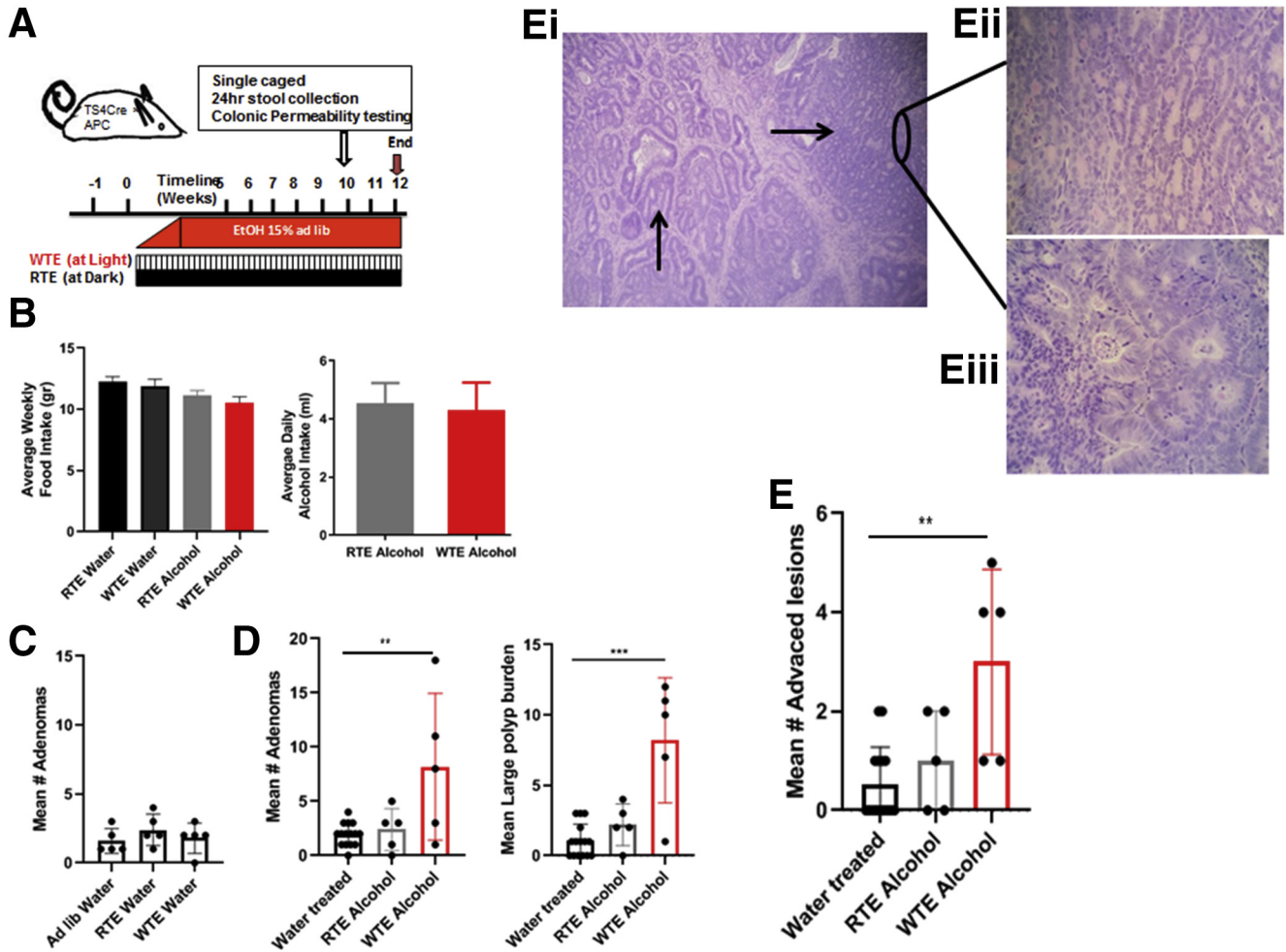


**Figure 2. Wrong-time eating interacts with alcohol to promote polyposis.** (A) TS4/APC mice were given access to alcohol (15% in water) or water and access to standard chow ad libitum, during the dark period (RTE), or during the light period (WTE) ( $n = 5$  mice per treatment group). (B) Feeding protocol (RTE or WTE) did not affect average food or alcohol intake, and (C) did not impact polyp numbers in water-treated animals. (D) Compared with water-treated animals, WTE + alcohol mice had more polyps (tubular adenomas) (*left*), more large ( $\geq 1$  mm) polyps (*right*), and (E) advanced adenomas (ie, severe, high-grade dysplasia/carcinoma in situ). (Ei) Example of a  $10\times$  view of a tubular adenoma in a WTE + alcohol animal: *vertical arrow* indicates low-grade dysplasia; *horizontal arrow* indicates carcinoma in situ (high-grade dysplasia) changes with back-to-back glands and no intervening stroma (Eii,  $40\times$  view), and cribriforming glands with focal necrosis (Eiii,  $40\times$  view). Data are expressed as means  $\pm$  SD. \* $P < .05$ , \*\* $P < .01$ , \*\*\* $P < .001$ . Ad lib, ad libitum.

WTE + alcohol treatment group relative to both other treatments (WTE + alcohol vs control water,  $P = .059$ ; WTE + alcohol vs RTE + alcohol,  $P = .035$ , unpaired  $t$  test) (Figure 3C). A similar level of within-treatment variability in the microbial community was observed for control water and RTE + alcohol treatments ( $P = .800$ , unpaired  $t$  test). In addition, microbial community structure was most similar between animals in control water and RTE + alcohol treatments, as assessed by between-group Bray-Curtis similarity (Figure 3C). Conversely, the similarity of microbial community structure was lowest between RTE + alcohol treatments and WTE + alcohol treatments (Figure 3C). The ratio of putative butyrate-producing genera to total putative SCFA-producing genera was decreased significantly in WTE + alcohol mice relative to mice from both other treatment groups (Kruskal-Wallis:  $P < .007$ ),

indicating a significant feeding effect (Figure 3D). The decrease in SCFA-producing bacterial abundance was consistent with direct metabolite measurements because WTE + alcohol mice showed a reduction in the absolute as well as the relative abundance of cecum butyrate levels (ratio of butyrate to total SCFAs) compared with the control water group (Figure 3E). The relative abundance of cecum butyrate levels could be an indicator of colonic butyrate production. Butyrate is taken up by the colonocytes as a cellular energy source, and the absolute fecal butyrate are not reflective of actual amounts being produced by the butyrate producers at the mucosal surface of the colon.<sup>27</sup>

### Intestinal Dysbiosis Precedes Polyposis

Next, we determined whether the observed dysbiosis preceded or followed polyposis by subjecting mice to shorter

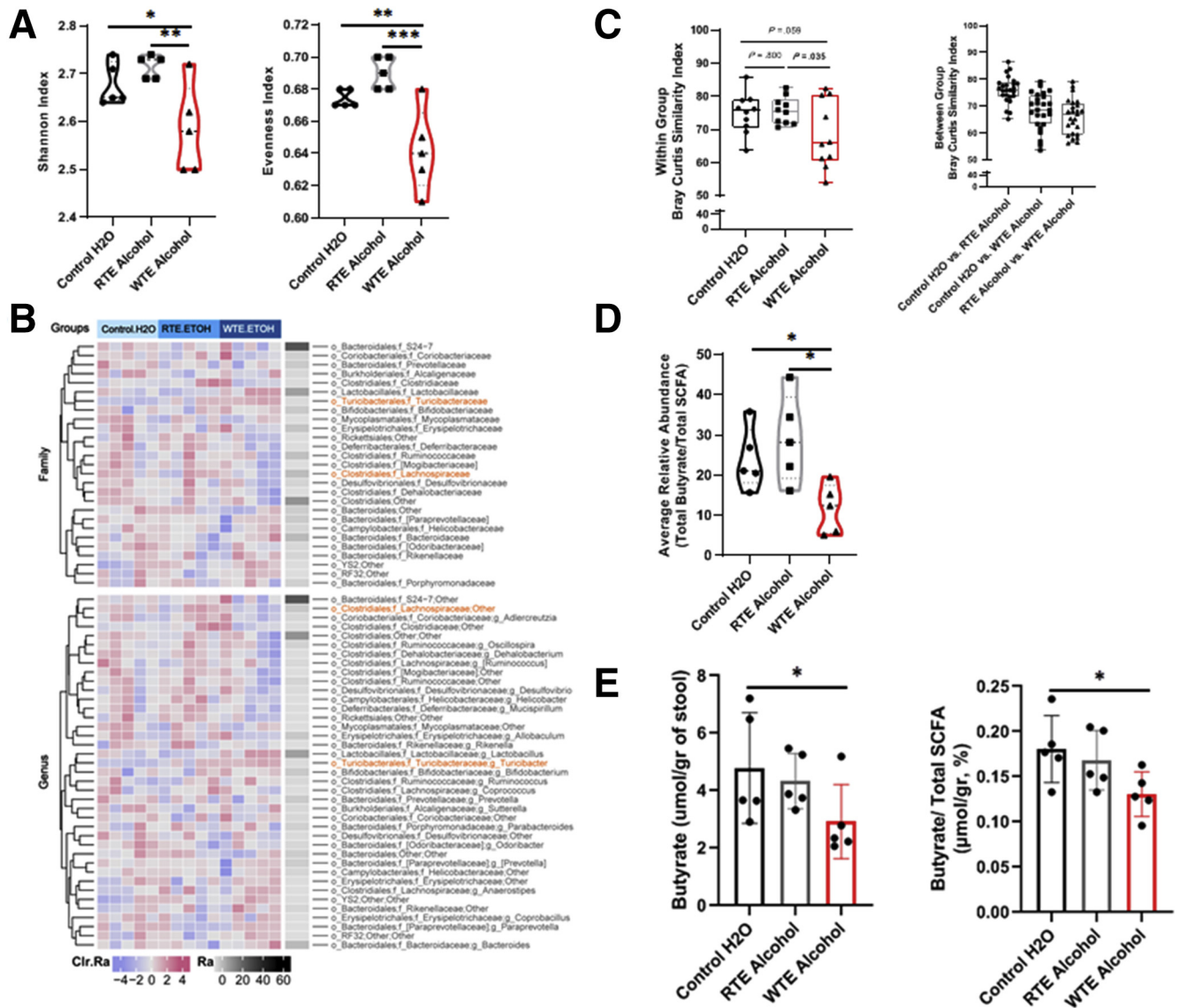


**Figure 3. Wrong time eating plus alcohol induces dysbiosis in TS4/APC mice.** (A) Fecal microbiome  $\alpha$  diversity as measured by 16S ribosomal RNA gene amplicon sequencing across treatments at the taxonomic level of genus. Analysis of the Shannon Index (1-way ANOVA:  $P = .014$ ) and evenness (1-way ANOVA:  $P = .002$ ) indicated a significant feeding effect across all 3 groups, with WTE + alcohol group diversity measures significantly lower than the other groups (\* $FDR < 0.05$ , \*\* $FDR < 0.01$ , \*\*\* $FDR < 0.001$ ). (B) Heatmap of differential taxon relative abundances at the taxonomic levels of family and genus (Kruskal–Wallis test on centered log ratio transformed data). No taxa were significantly different ( $FDR < 0.05$ ), however, the relative abundances of Lachnospiraceae families trended lower (Kruskal–Wallis centered log ratio transformed [CLR]:  $P = .025$ ) and Turcibacteraceae higher (Kruskal–Wallis CLR:  $P = .007$ ) across treatment groups, specifically in WTE + alcohol compared with both control water and RTE + alcohol mice ( $P < .05$ ). (C) Distribution of within-group Bray–Curtis similarity (taxonomic level of genus) of samples within each treatment group. Greater within-treatment variability was observed in animals in the WTE + alcohol treatment relative to animals within both other treatments (WTE + alcohol vs control H<sub>2</sub>O,  $P = .059$ ; WTE + alcohol vs RTE + alcohol,  $P = .035$ , unpaired  $t$  test). Between-group Bray–Curtis similarity was calculated for pairwise comparisons of all 3 treatment groups. Microbial communities were most similar between animals of the control H<sub>2</sub>O group and RTE + alcohol, whereas those of the RTE + alcohol and WTE + alcohol groups were most dissimilar. (D) The relative abundance of total butyrate-producing genera to all SCFA-producing genera was significantly different across treatment groups (Kruskal–Wallis:  $P = .007$ ), with a decrease in WTE + alcohol compared with control water and RTE + alcohol mice (\* $FDR < 0.05$ ). (E) Measurement of SCFA metabolite levels in stool as the butyrate level per gram of stool (left) as well as the ratio of butyrate-to-total SCFA concentrations (right). Data are expressed as means  $\pm$  SD for  $n = 5$  mice per treatment group \* $P < .05$ .

durations (for 6 and 8 weeks) of WTE + alcohol treatment in a time course experiment (Figure 4A). Compared with control water, WTE + alcohol mice showed increased numbers of tumors only after 12 weeks, but not after 6 or 8 weeks of

treatment (Figure 4B). The effect of the WTE + alcohol regimen on the overall microbial community structure, however, was observed by week 6 (ANOSIM:  $R = 0.632$ ;  $P = .016$ ), and also was observed at week 8 (ANOSIM:  $R = 0.292$ ;

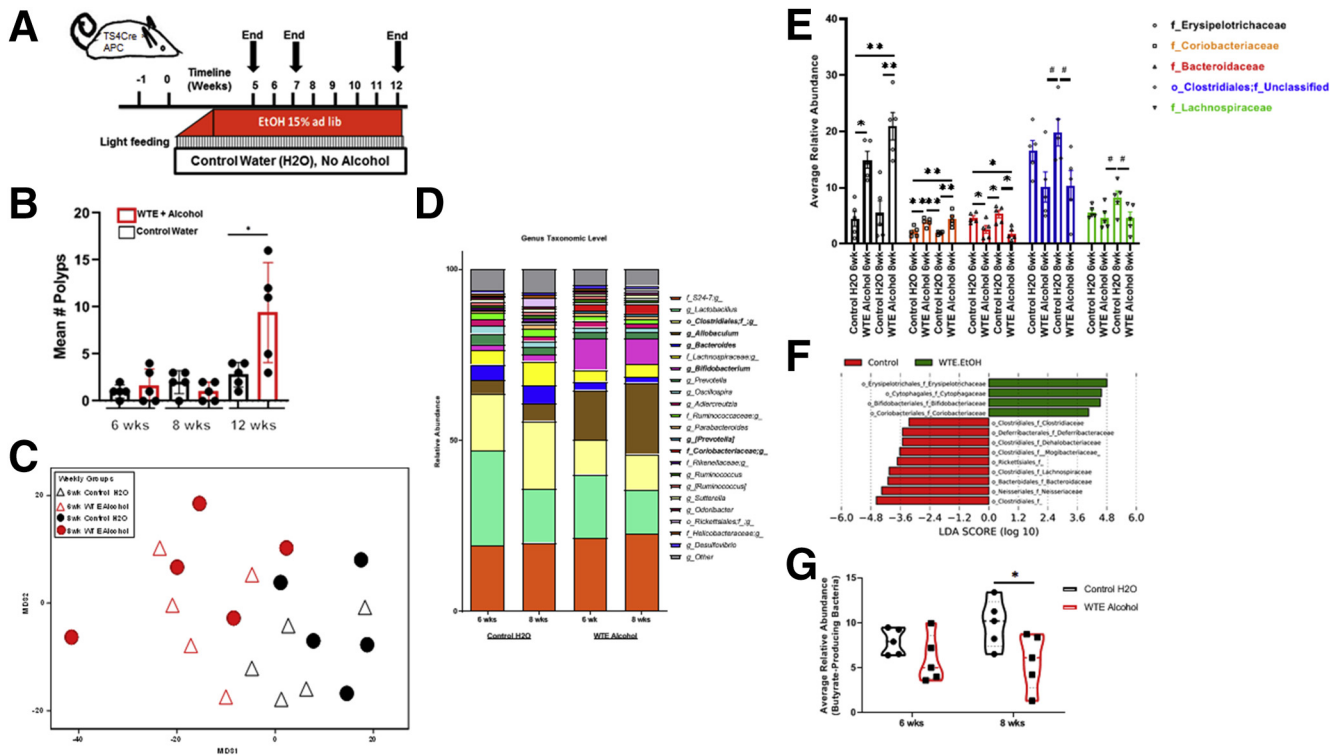


**Figure 4. Dysbiosis in wrong time eating plus alcohol TS4/APC mice precedes polyposis.** (A) TS4/APC mice were given access to standard chow and alcohol (15% in water) with a light-period feeding schedule (WTE + alcohol) or feeding access to chow but no alcohol (control water) for the indicated periods of time. (B) The total number of tubular adenomas were compared at treatment completion  $*P < .05$ . (C) Multidimensional scaling (MDS) plot of fecal microbial community structure from treatment groups at weeks 6 and 8 (taxonomic level of genus). A significant effect of treatment was observed as early as week 6 (ANOSIM: global  $R = 0.632$ ;  $P = .016$ ), and was maintained at week 8 (ANOSIM: global  $R = 0.292$ ;  $P = .024$ ). (D) Stacked column plots depicting the average number of rarefied microbial reads ( $>1\%$ ) at the genus level, between WTE + alcohol and control water mice at weeks 6 and 8, with significantly different taxa bolded (FDR  $< 0.05$ ). (E) Average relative abundance for family level taxa that were significantly different between treatment groups. Significance was assessed using the Kruskal-Wallis test on centered log ratio transformed data: WTE + alcohol had higher relative abundances of Erysipelotrichaceae (FDR:  $P = .030$ ) and Coriobacteriaceae (FDR:  $P = .030$ ); WTE + alcohol had lower relative abundances of Bacteroidaceae (FDR:  $P = .036$ ), Clostridiales unclassified ( $P = .045$ ), and Lachnospiraceae ( $P = .047$ ). Multiple-group comparison between the 4 mice time groups are indicated ( $*FDR < 0.05$ ,  $**FDR < 0.01$ ,  $\#P < .05$ ). (F) Linear discriminant analysis (LDA) effect size results showing which microbial taxa (family level) most likely explain differences between WTE + alcohol and control water, across both weeks 6 and 8 samples. (G) Average relative abundance of total butyrate-producing genera at 6 and 8 weeks. A 2-way ANOVA (treatment:  $P < .016$ ) with multiple-comparison FDR correction (week 8:  $*FDR < 0.05$ ) was used to determine significance. Data are expressed as means  $\pm$  SD for  $n = 5$  mice per treatment group.

$P = .024$ ) (Figure 4C, Table 1). The interaction effect of time and treatment on genus-level taxonomic richness was significant at week 8 in WTE + alcohol animals (2-way ANOVA:  $F_{(1,16)} = 4.933$ ,  $P = .041$ ; week 8: FDR = 0.021) (Table 2). The effects of the WTE + alcohol regimen over time on individual taxa are shown at the taxonomic level of genus (Figure 4D). Differential abundances of individual family level taxa across time and multiple group comparisons were assessed (Figure 4E). The relative abundance of Erysipelotrichaceae (FDR = 0.030) and Coriobacteriaceae (FDR = 0.030) was significantly higher in WTE + alcohol mice relative to control animals. Conversely, the relative abundance of Bacteroidaceae (FDR = 0.036), Clostridiales unclassified ( $P = .045$ ), and Lachnospiraceae ( $P = .047$ ) were significantly or trending lower in WTE + alcohol mice relative to control animals. We also used the software package Linear Discriminant Analysis Effect Size to identify significant microbial features

most associated with feeding and strongly differentiating microbial communities in control water vs WTE + alcohol treatments across all time (Figure 4F). Finally, a decrease in the overall relative abundance of total putative butyrate-producing genera was observed in feces from WTE + alcohol animals relative to control animals (2-way ANOVA:  $F_{(1,16)} = 7.335$ ,  $P = .016$ ; week 8: FDR = 0.020) (Figure 4G). These results suggest dysbiosis as marked by reductions in the levels of butyrate-producing bacteria preceded exacerbation of tumorigenesis.

### Prebiotic Treatment Corrects Dysbiosis, Increases Butyrate Levels, and Decreases Polyposis in WTE + Alcohol Mice

We hypothesized that targeting dysbiosis to improve butyrate production would ameliorate WTE +

**Table 1.** Group ANOSIM Results for Mouse Fecal Microbiota Compositions Between Weeks 6 and 8 Control Water and Wrong Time Eating Alcohol, at the Genus Taxonomic Level

Comparison	Taxonomic level	Global <i>R</i>	<i>P</i> value <sup>a</sup>
Between-week comparison: control water 6- vs 8-week control water	Genus	0.180	.127
Between-week comparison: WTE alcohol 6- vs 8-week WTE alcohol	Genus	-0.02	.524
Across-treatment comparisons			
6 weeks: control water vs WTE alcohol	Genus	0.632	<b>.016</b>
8 weeks: control water vs WTE alcohol	Genus	0.292	<b>.024</b>

NOTE. Twenty total fecal samples for analysis; the number of fecal samples per time point/per group = 5; collection weeks: 6 and 8. Boldface indicates statistical significance.

<sup>a</sup>*P* < .05, global *R* comparison was based on ANOSIM and *P* values were calculated based on a permutational analysis, using 126 permutations. Data were square-root transformed.

alcohol-associated tumorigenesis. TS4/APC mice were subjected to the WTE + alcohol regimen with or without TD160445, a prebiotic that increases SCFA-producing bacterial levels<sup>28</sup> (Figure 5A). Without impacting weight or alcohol intake (Figure 5B), prebiotic TD160445 significantly affected the overall microbial community structure in WTE + alcohol mice (ANOSIM: *R* = 0.512; *P* = .016) (Figure 5C). No significant differences between  $\alpha$  diversity indices between the 2 treatment conditions were observed (data not shown). The overall relative abundances of microbial taxa (>1%;

taxonomic level of genus) between the 2 mice groups is shown in Figure 5D. The prebiotic TD160445 increased the relative abundance of bacteria from the SCFA-producing genus *Bifidobacterium* (*P* = .009) in WTE + alcohol mice (Figure 5E). The average relative abundance of total butyrate-producing genera to total SCFA-producing genera taxa increased (Mann-Whitney *U* test: *P* = .032) in the WTE + alcohol mice after TD160445 treatment (Figure 5F).

Metabolite analysis confirmed that TD160445 significantly increased relative butyrate levels (Figure 5G),

**Table 2.** Effect of Treatment and Time on Mouse Fecal  $\alpha$  Diversity Indices at Different Taxonomic Levels (Control Water and Wrong Time Eating + Alcohol) at Weeks 6 and 8

Taxonomic level $\alpha$ diversity	Interaction <sup>a</sup>	Treatment <sup>a</sup>	Time <sup>a</sup>	Time point comparisons <sup>b</sup>
Phylum Shannon	0.218	0.097	0.363	NS
Phylum Simpson	0.370	0.067	0.412	NS
Phylum Richness	0.360	1.000	0.360	NS
Phylum Evenness	0.137	0.112	0.339	NS
Class Shannon	0.410	<b>0.008</b>	0.835	<b>Week 6*</b>
Class Simpson	0.844	<b>0.005</b>	0.743	NS
Class Richness	0.191	0.103	0.424	NS
Class Evenness	0.207	<b>0.024</b>	0.886	<b>Week 6*</b>
Order Shannon	0.426	<b>0.008</b>	0.800	<b>Week 6*</b>
Order Simpson	0.897	<b>0.005</b>	0.796	NS
Order Richness	<b>0.046</b>	0.231	0.557	NS
Order Evenness	0.109	<b>0.021</b>	1.000	<b>Week 6*</b>
Family Shannon	0.200	0.309	0.505	NS
Family Simpson	0.333	1.000	0.333	NS
Family Richness	<b>0.016</b>	0.345	0.383	<b>Week 8*</b>
Family Evenness	0.082	0.220	0.649	NS
Genus Shannon	0.239	0.337	0.656	NS
Genus Simpson	0.306	0.897	0.518	NS
Genus Richness	<b>0.041</b>	0.173	0.538	<b>Week 8*</b>
Genus Evenness	0.138	0.269	0.759	NS

NOTE. Twenty total fecal samples for analysis; the number of fecal samples per time point/per group = 5; collection weeks: 6 and 8. Boldface indicates statistical significance.

<sup>a</sup>Two-way ANOVA: *P* < .05, factors included interaction, treatment, time.

<sup>b</sup>False discovery rate multiple comparisons: \**P* < .05 for FDR time point comparisons.

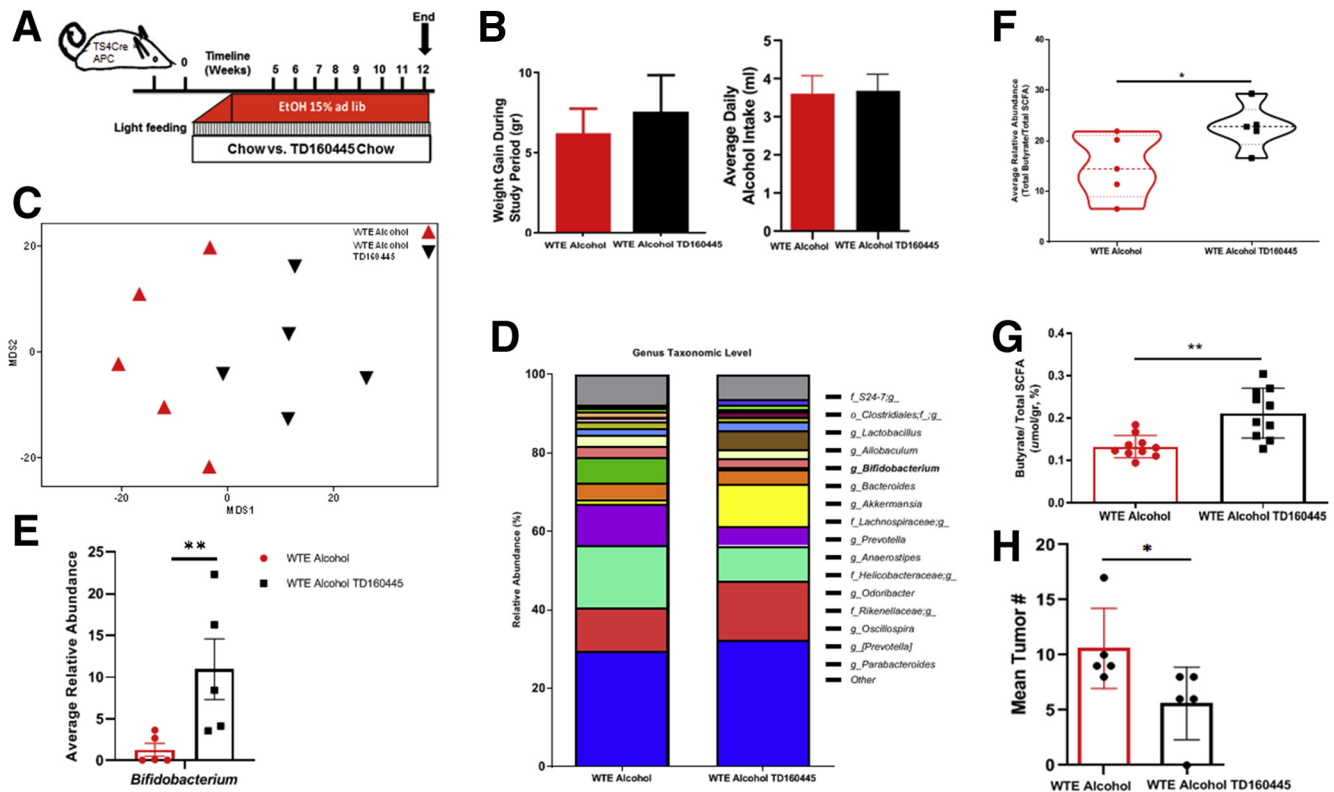


**Figure 5. TD160445 treatment changes microbial structure, corrects dysbiosis, increases butyrate levels, and ameliorates polyposis in WTE-alcohol TS4/APC mice.** (A) TS4/APC mice were given access to alcohol (15% in water) and standard or prebiotic TD160445-containing chow using a light-period feeding schedule. (B) TD160445 administration did not affect average weight gain or alcohol intake of the mice over the study period. (C) Multidimensional scaling (MDS) plot of fecal microbial community structure shows a significant effect of TD160445 (ANOSIM:  $R = 0.512$ ,  $P = .016$ ; taxonomic level of genus). (D) TD160445 affects microbial taxa: stacked column plots depicting the average number of rarefied microbial reads (>1%), with significantly different taxa bolded ( $P < .05$ ) between WTE + alcohol + chow and WTE + alcohol + TD160445 mice, at the genus level. (E) The average relative abundance of the *Bifidobacterium* genus was significantly higher in mice fed prebiotic TD160445 (Kruskal-Wallis centered log ratio transformed:  $P = .009$ ). (F) Mice fed the prebiotic TD160445 had significantly higher average relative abundances of total butyrate-producing genera (Mann-Whitney  $U$  test:  $P = .032$ ). (G) The ratio of total butyrate-to-total SCFA metabolites, as measured by gas chromatography, was significantly higher in fecal samples after TD160445 treatment (Mann-Whitney  $U$  test:  $P < .01$ ). (H) Number of tumors, as assessed by determining the number of formed polyps was decreased in the prebiotic-treated group (Mann-Whitney  $U$  test:  $P < .05$ ). Data are expressed as means  $\pm$  SD for  $n = 5$  mice per treatment group. \* $P < .05$ , \*\* $P < .01$ .

indicating comparatively higher colonic butyrate production during prebiotic treatment. Moreover, the prebiotic treatment significantly reduced tumor numbers in the WTE + alcohol mice (Figure 5H).

### Dysbiosis From Rest-Time Food and Alcohol Access Coincides With Colon Inflammation

Butyrate has been proposed to modulate colon carcinogenesis, in part via induction of colonic FOXP3<sup>+</sup> T cells and dampening of intestinal inflammation.<sup>25,26</sup> Mucosal inflammatory processes in the colon compromise mucosal barrier function, resulting in increased intestinal permeability, which has been implicated in carcinogenesis.<sup>29,30</sup> Intestinal permeability also is promoted by alcohol and CRD.<sup>13</sup>

To test whether the observed exacerbated polyposis was associated with a hyperpermeable state, we estimated colonic permeability by measuring sucralose excretion in

urine.<sup>31</sup> Compared with control water, WTE + alcohol mice showed higher sucralose excretion (Figure 6A), indicating impaired mucosal permeability that potentially increased permeation of luminal proinflammatory factors, resulting in mucosal immune dysregulation or inflammation.<sup>32</sup>

Enhanced lymphocytic infiltration in CRC has been associated with a favorable clinical prognosis,<sup>33,34</sup> with effector T cells thought to invade cancerous tissue. To characterize the overall lymphocytic profile in our model, we assessed the abundance of total CD3<sup>+</sup>, as well as of CD4<sup>+</sup>, lymphocytes. We observed reduced polyp infiltration by CD3<sup>+</sup> T cells, both in their overall and relative abundance to CD4<sup>+</sup> cells, in the WTE + alcohol group (Figure 6B and C), consistent with increased inflammation and a weakened effector T-cell profile reported in CRC.<sup>35,36</sup> There was a significant effect of alcohol ( $F = 27.1$ ;  $P < .01$ ) and a positive interaction between alcohol and WTE ( $F = 8.4$ ;  $P < .01$ ) in reducing the densities of colon-infiltrating CD3<sup>+</sup>



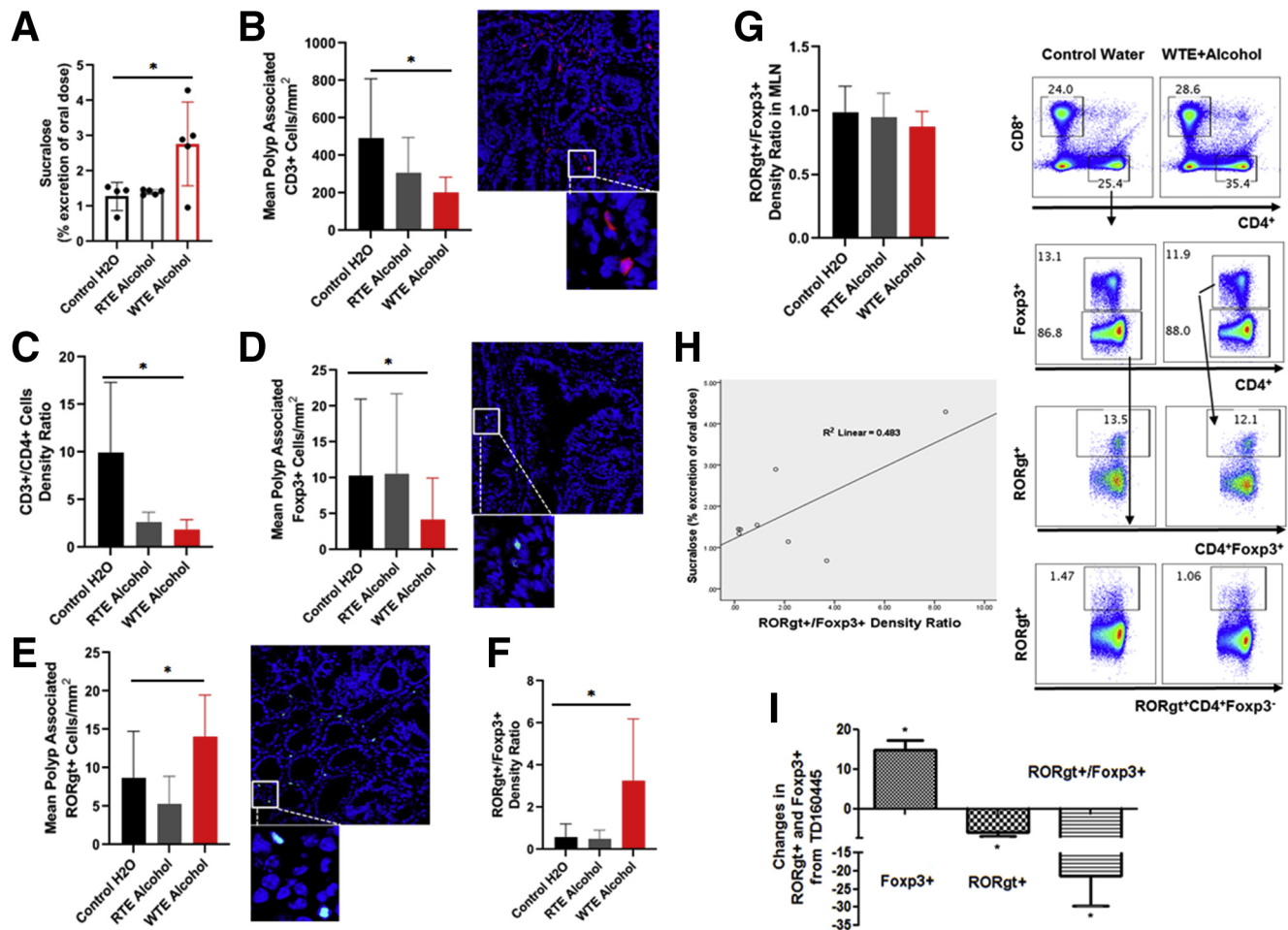


**Figure 6. Rest-time food and alcohol access promote tumor-associated inflammation.** (A) Colon permeability increased in WTE + alcohol mice using urine excretion ratios of sucralose. (B and C) By using immunofluorescence, (B) polyp-associated CD3<sup>+</sup> cell density per surface area as well as (C) the CD3<sup>+</sup>/CD4<sup>+</sup> cell density ratio was determined for each polyp and compared between the groups. (D and E) The density of (D) FOXP3<sup>+</sup> and (E) RORγt<sup>+</sup> cells in the peripolyp surface areas was lower and higher, respectively, in the WTE + alcohol mice vs the control water group (N = 99 polyp images were used for quantification). Representative stained slide images are shown for (B) CD3, (D) FOXP3, and (E) RORγt at 20× magnification, with the inset at 40× magnification. Between-group comparisons of the RORγt<sup>+</sup>/FOXP3<sup>+</sup> ratio in the (F) mucosa and (G) mesenteric lymph nodes as determined by flow cytometry are shown. Representative gating scheme of 1 mouse for CD4<sup>+</sup> T-cell intracellular FOXP3 and RORγt cytometry is shown. No significant differences in FOXP3<sup>+</sup> and RORγt<sup>+</sup> T-cell abundance were observed among the tested groups. (H) Correlation between the urine excretion ratio of sucralose and the polyp-associated RORγt<sup>+</sup>/FOXP3<sup>+</sup> ratio. (I) TD160445 treatment increased mucosal FOXP3<sup>+</sup> and decreased RORγt<sup>+</sup> cell density, as well as the RORγt/FOXP3<sup>+</sup> ratio in WTE + alcohol-treated mice (N = 48 polyp images were used for the quantification of the 2 groups in the prebiotic experiment). \*P < .05. MLN, mesenteric lymph node.

cells. Thus, the higher colonic permeability in WTE + alcohol mice correlated with increased inflammation and an overall lower effector profile in the polyp mucosa.

### *Dysbiosis in WTE + Alcohol Mice Affects the Balance Between T-Helper 17 Cells and Regulatory T Cells*

CRC is characterized by a proinflammatory state, with higher densities of proinflammatory T-helper 17 (Th17) cells and a lower abundance of regulatory T cells (Tregs).<sup>37–41</sup> Extrathymically induced FOXP3<sup>+</sup> Tregs (eTregs) are influenced by the intestinal microbiota and by the respective bacterial metabolites, including butyrate.<sup>25,26</sup>

Butyrate-producing bacteria are among the strongest inducers of eTregs.<sup>42,43</sup> Considering the reduced levels of butyrate and butyrate-producing bacteria and increased colonic permeability, we next tested whether polyposis in the WTE + alcohol mice was associated with a CRC-like immune profile in the mucosa. By using immunofluorescent staining, we quantified polyp-infiltrating FOXP3<sup>+</sup> Treg and Retinoic Acid Receptor (RAR)-related orphan receptor γ-positive (RORγt<sup>+</sup>) Th17 cell densities. Relative to control, WTE + alcohol mice harbored significantly lower densities of polyp-infiltrating Tregs, higher Th17 densities, and an increased RORγt/FOXP3 ratio (Figure 6D–F). However, the abundance of FOXP3<sup>+</sup> and RORγt<sup>+</sup> cells, as well as the RORγt/FOXP3 ratio, in the mesenteric lymph nodes was

comparable in all experimental groups (Figure 6G). These results suggest that the inflammatory changes occur mainly at the tumor sites within the mucosa, further underscored by a significant correlation between the polyp-associated ROR $\gamma$ t/FOXP3 ratio and intestinal permeability (Figure 6H).

### Microbial Recovery Resets the Mucosal Immune Profile

We next examined whether recovery of relative butyrate levels suppressed the proinflammatory profile of WTE + alcohol mice. TD160445 prebiotic significantly increased tumor-associated Treg densities and decreased the ROR $\gamma$ t/FOXP3 ratio in WTE + alcohol mice (Figure 6I). Thus, correction of the microbiota profile by TD160445 (Figure 5C–F) restored relative butyrate levels in the colon (Figure 6H), resetting the pathogenic immune environment and decreasing tumorigenesis.

### Butyrate Signaling and the Proinflammatory Circuit Are Linked in Polyposis-Prone WTE + Alcohol Mice

SCFAs regulate mucosal inflammation and carcinogenesis in part via G-protein-coupled receptor (GPR) signaling.<sup>44,45</sup> Expression of GPR109A, a butyrate receptor that plays a protective role in colonic inflammation and CRC,<sup>46,47</sup> was lowest in WTE + alcohol TS4/APC mice (Figure 7A). Expression of another butyrate receptor, GPR43, also decreased in this group, but not significantly (Figure 7A). These results were consistent with decreased butyrate signaling in WTE + alcohol mice. In addition, with GPR109A inducing the differentiation of CD4<sup>+</sup> T cells into FOXP3<sup>+</sup> Tregs,<sup>46</sup> the reduced expression of GPR109A was consistent with the reduced abundance of polyp-associated FOXP3<sup>+</sup> cells in WTE + alcohol mice. The lack of effect on mesenteric lymph node Treg abundance (Figure 6G) indicates local and tumor-specific GPR109A effects. Immunostaining confirmed reduction of GPR109A expression within the polyp and polyp margins relative to distant healthy colon tissue (Figure 7B), consistent with the proposed tumor-suppressive role of butyrate stimulation of GPR109A.<sup>47</sup>

Excessive signal transducer and activator of transcription 3 (STAT3) activity reduces Treg recruitment, dysregulates mucosal immunity, and promotes colon carcinogenicity.<sup>48</sup> Staining for phosphorylated STAT3 indicated enhanced epithelial STAT3 activation in WTE + alcohol mice (Figure 7C), consistent with a potential link between STAT3 epithelial signaling and the tumor-associated immune imbalance in these polyposis-prone mice. Knockdown of GPR109A in Caco2 colon epithelial cells increased nuclear phosphorylated STAT3 levels (Figure 7D). STAT3 activation upon GPR109A knockdown decreased Chemokine ligand (CCL)28 (Figure 7D), a STAT3-regulated epithelial chemokine that is involved in Treg recruitment.<sup>48</sup> These results suggest that loss of GPR109A in the colon of WTE + alcohol polyposis-prone mice likely is linked mechanistically to increased inflammation and colon carcinogenesis.

### Butyrate Signaling and Proinflammatory Profiles Are Linked in Human CRC

We next assessed whether our findings are pertinent to human CRC by analyzing data available in The Cancer Genome Atlas. A negative correlation between the expression of genes encoding ROR $\gamma$ t (*RORC*) and FOXP3 (*FOXP3*) in human CRC support their opposing effects on colon carcinogenesis (Figure 7E). Furthermore, GPR109A-encoding *HCAR2* messenger RNA levels correlated inversely with *RORC* expression (Figure 7F) and positively with *FOXP3* expression (Figure 7G). These results support the inverse correlation between butyrate signaling and a proinflammatory profile in human CRC.

## Discussion

CRC is among the top causes of cancer-related deaths worldwide.<sup>1,2</sup> Although screening has reduced CRC rates in older populations in developed countries, younger adults currently are experiencing a rapid increase in CRC rates, likely owing to lifestyle habit changes.<sup>2</sup> Epidemiologic studies have supported a clinical association between environmental risk factors and CRC,<sup>5</sup> with elements of the modern lifestyle causing pathogenic inflammation, which in turn facilitates colonic tumorigenesis.<sup>9,29,30</sup> The intestinal microbiota and associated metabolites further mediate environmental effects on colon inflammation and CRC.<sup>1,49</sup>

CRD, a common aspect of the modern lifestyle in our 24-hours/7-days-a-week society, has long been overlooked as a risk factor for a variety of chronic diseases including cancer.<sup>15,16</sup> We previously showed that CRD induced by altering the light/dark cycles promoted mucosal inflammation in an animal model of colitis.<sup>50</sup> When combined with alcohol consumption, CRD promoted dysbiosis, intestinal hyperpermeability, and inflammation,<sup>13</sup> with light/dark shifts enhancing alcohol-induced CRC.<sup>17</sup>

Despite much focus on light/dark phase shifts, other forms of CRD have not been widely studied. Eating near or during the physiologic rest time is a common habit in our society. Dinner tends to be the highest-calorie-containing meal more than 4 times per week among healthy individuals in the United States.<sup>20</sup> Consistent with earlier findings showing that time-restricted feeding dissociates central and peripheral liver and colon clocks,<sup>18,19</sup> our data showed that eating during the rest phase can cause CRD by dissociating central and colonic rhythms.

To assess the interaction of WTE with alcohol consumption in facilitating protumorigenic colon inflammation and carcinogenesis, we used a polyposis model that mimics human CRC and allows analysis of the colon microbiota. We showed a positive interaction of alcohol with WTE in colon polyposis and carcinoma development. The exacerbated tumorigenesis was associated with a hyperpermeable state, reduced polyp infiltration by CD3<sup>+</sup> T cells both in their overall and relative abundance to CD4<sup>+</sup> cells, lower polyp-associated densities of Tregs, and an increased ROR $\gamma$ t/FOXP3 ratio. Alcohol and WTE reduced the levels of butyrate-producing bacteria and consequently of butyrate levels in the colon. The associated intestinal

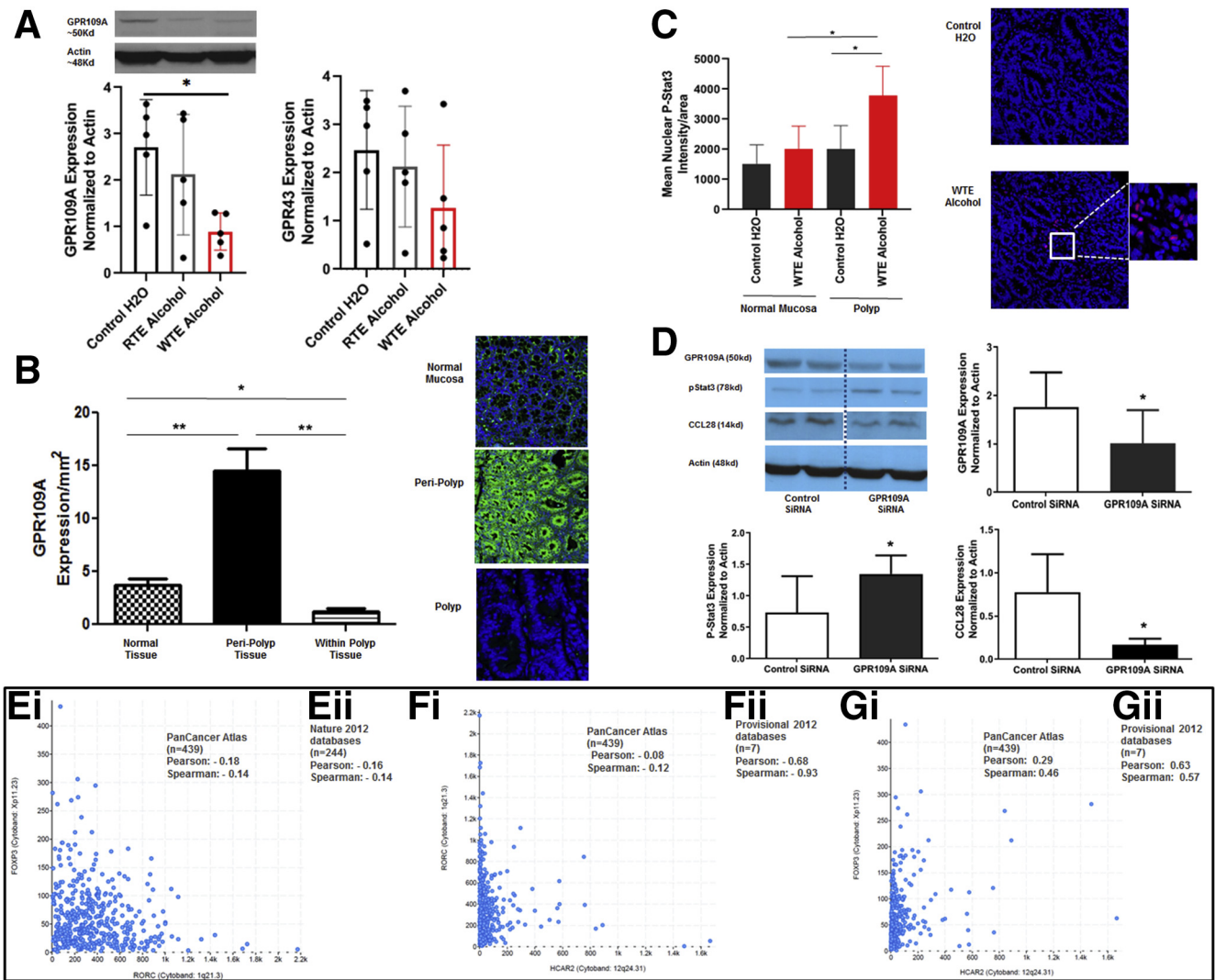


**Figure 7. Reduced butyrate signaling is associated with a proinflammatory circuit in wrong time eating plus alcohol mice, as well as in human colorectal cancers.** (A) Normalized GPR109A and GPR43 protein levels in the proximal colon tissue of WTE + alcohol TS4/APC mice were determined using immunoblotting. A representative GPR109A Western blot is shown. Quantification includes  $n = 5$ /group. (B) Tissue distribution of GPR109A in the proximal colon of TS4/APC mice was assessed using immunofluorescence staining; a  $20\times$  magnification representative image per field is shown. Quantification was performed on 20 size-matched polyps, peripolyps, and normal areas of TS4/APC mice proximal colon; 3 images per area were used for quantification. (C) Immunofluorescence staining for phosphorylated STAT3 (p-STAT3) showed increased nuclear p-STAT3 levels in polyp epithelial cells of WTE + alcohol relative to control water/H<sub>2</sub>O mice. Representative images show  $20\times$  magnification of the polyp area. Bars represent the average positive p-STAT3 nuclear signals per area. For each group, 17 tumors were imaged, and 3–5 images from each tumor and peritumor area were quantified. (D) GPR109A was knocked down in Caco2 cells using small interfering RNA (SiRNA) (see the [Materials and Methods](#) section). Expressions of P-Stat3 and CCL28 was assessed by Western blot; P-Stat3 and CCL28 expression was quantified after normalization to actin in GPR109A-deficient and GPR109A-proficient cells (results of 3 independent experiments were used for quantification). *ROR* $\gamma$ *t*/*FOXP3* status and *GPR109A* expression in human colorectal cancers: inverse correlation between gene expressions of *FOXP3* and *RORC* is seen in (Ei) 439 cases from the PanCancer Atlas and (Eii) 244 cases from the Nature 2012 databases. (F and G) *GPR109A* (*HCAR2*) gene expression is correlated with the proinflammatory (*ROR* $\gamma$ *t*<sup>+</sup>/*FOXP3*<sup>+</sup>) profile. (Fi and Fii) Inverse correlation between *RORC* and *HCAR2* gene expression, and (Gi and Gii) positive correlation between *FOXP3* and *HCAR2* gene expression. The data and graph were from The Cancer Genome Atlas. Graphs that were generated from the PanCancer Atlas database are shown. \* $P < .05$ , \*\* $P < .01$ .

hyperpermeability and mucosal inflammation in the colon of polyp-prone WTE + alcohol mice was dampened by TD160445, a prebiotic that expands butyrate-producing bacterial populations.<sup>28</sup> Inference of functional differences using predictive assessment of the microbial community

functional potential also showed a significant decrease in inferred metagenome SCFA pathways in the WTE + alcohol group relative to other treatments (FDR < 0.05), and an increase in 9 predicted SCFA pathways in response to TD160445 (data not shown).

Mucosal inflammation in WTE + alcohol mice coincided with lower FOXP3<sup>+</sup> and higher ROR $\gamma$ t<sup>+</sup> cell abundances. FOXP3<sup>+</sup> Tregs suppress proinflammatory cytokine production by other immune cells, such as ROR $\gamma$ t<sup>+</sup> cells.<sup>51</sup> During early carcinogenesis, Tregs can suppress proinflammatory immune cells.<sup>24</sup> High FOXP3<sup>+</sup> and low ROR $\gamma$ t<sup>+</sup> cell densities within tumors are associated with improved survival of CRC patients.<sup>37,38,52,53</sup> The Cancer Genome Atlas analysis confirmed the inverse correlation between *FOXP3* and *RORC* expression in human CRC.

Despite defending against pathogens, intestinal immunity also can promote tumorigenic inflammatory processes. Longitudinal maintenance of mucosal immunity balance depends on microbiota-driven signaling,<sup>25,26</sup> with bacteria-derived SCFAs<sup>44,54</sup> maintaining mucosal immune homeostasis.<sup>44,54,55</sup> In particular, butyrate signaling through GPR109A induces FOXP3<sup>+</sup> Tregs in the intestine,<sup>46</sup> with butyrate dampening polyposis.<sup>46</sup> Our data showed that the proinflammatory bacterial profile and exacerbated polyposis in WTE + alcohol mice could be driven at least in part by a reduction in butyrate-producing bacterial populations.

Both alcohol and CRD can cause intestinal dysbiosis.<sup>56–61</sup> We observed that alcohol-induced dysbiosis is augmented by WTE. Microbial changes were associated with decreased levels of relative abundance of butyrate-producing bacteria and of its receptor GPR109A in the colon of WTE + alcohol mice. Reduced abundance of butyrate-producing bacteria preceded exacerbated polyposis. Microbiota recovery using the prebiotic TD160445 restored the colonic butyrate levels, reset the environment, and decrease tumorigenesis. Previously, probiotic treatment also was shown to increase FOXP3<sup>+</sup> Treg and decrease ROR $\gamma$ t<sup>+</sup> proinflammatory cell levels, reducing colon polyposis.<sup>62</sup> Our present prebiotic data have potentially important clinical implications considering the correlations between *HCAR2*, *RORC*, and *FOXP3* expression in human CRCs.

Butyrate-GPR109A signaling can induce differentiation of intestinal FOXP3<sup>+</sup> Tregs through innate immune cells, such as macrophages and dendritic cells.<sup>46</sup> Treg numbers also can be boosted by butyrate via epigenetic-dependent differentiation of eTregs.<sup>26</sup> Presently, we observed no significant changes in Treg numbers in the lymph nodes draining the proximal colon where polyposis occurred. Furthermore, we observed no variation in FOXP3<sup>+</sup> cell densities in normal non-polyp-bearing mucosa between different treatment groups. These findings suggest that the polyp-associated proinflammatory profile in our model, despite butyrate responsiveness, likely depends on recruitment rather than an overall differentiation of FOXP3<sup>+</sup> cells at the intestinal level. We observed increased STAT3 activation in polyp epithelial cells of WTE + alcohol mice.

STAT3 activation reduces FOXP3<sup>+</sup> Treg recruitment by inhibiting expression of Treg-recruiting chemokines, including CCL19, CCL28, and CCL5, and promotes tumor progression by inducing mucosal immune dysregulation.<sup>48</sup> We found that decreased GPR109A expression in the colon epithelium led to increased activation of STAT3, and decreased CCL28. In vivo, expression of GPR109A was lowest in WTE + alcohol TS4/APC mice consistent with the

loss of Treg cells and enhanced epithelial STAT3 activation in this group. However, it is unclear whether butyrate can affect epithelial STAT3 via GPR109A-independent pathways. These data suggest that microbiota-derived butyrate inhibits STAT3 activation, improving the tumor-associated effector profile.

Our results show a novel role for eating times in inducing CRD and in promoting alcohol-associated colonic inflammation and tumorigenesis. This interaction is particularly important because circadian misalignments and alcohol use disorders are increasing and commonly are associated with young individuals.<sup>63</sup> This interaction promotes colon carcinogenesis by inducing a protumorigenic mucosal inflammatory profile, at least in part by altering the intestinal butyrate levels.

In addition to SCFA, several studies have shown the potential importance of other bacterial metabolites in CRC. Indeed, several studies have suggested the importance of bile acids in carcinogenesis. However, we did not find any differences in the stool bile acid profiles between WTE + alcohol and the control water groups (Table 3). Nonetheless, our results do not preclude the role for other commensal bacteria or bacteria metabolites in mediating environmental effects on tumor immunity. Our findings also suggest that intersubject heterogeneity in alcohol-associated CRC risk may arise from predisposing factors such as CRD and variations in gut microbiome composition. Thus, microbial intervention represents a potential strategy for CRC prevention in individuals with a high-risk lifestyle profile. Additional studies are required to further characterize pathways linking bacterial metabolites with environment-modulated mechanisms driving carcinogenesis in the colon mucosa.

## Materials and Methods

### Animal Experiments

Unless otherwise indicated, all animals were acquired from Jackson Laboratories (Bar Harbor, ME) and bred and genotyped in-house. Animals, individually housed in cages inside ventilated light-tight cabinets, were maintained on a 12-hour light/dark cycle. Envigo 2018 standard rodent chow (Teklad, Madison, WI) was used as the animals' diet, unless otherwise specified. The time lights were turned on was referred to as Zeitgeber time (ZT)0, with lights turned off at ZT12. All experiments were conducted at Rush University Medical Center (Chicago, IL) with approval of the Institutional Animal Care and Use Committee.

### PER2::LUC reporter experiments

Eight-week-old B6 PER2:LUC mice were assigned randomly to a regular chow diet given during the dark (RTE, n = 5) or light (WTE, n = 5) periods (Figure 1). Locomotor activity was measured throughout the experiment using infrared beam breaks.<sup>13</sup> For PER2::LUC reporter activity monitoring, colons were harvested after cervical dislocation. After Krebs solution rinsing, four 2- to 3-mm<sup>2</sup> sections were excised and placed lumen-side-up onto an insert in luciferin-containing recording medium. Luciferase activity was monitored every 4 hours for 7 days

**Table 3.** Quantification and Comparison of Bile Acid Metabolites per Nanogram/Gram of Stool in Control Water Vs Wrong Time Eating + Alcohol

Bile acid metabolites, means $\pm$ SD	Treatment		P value	Significance <sup>a</sup>
	Control water	WTE + alcohol		
Sulfolithocholic acid	3.62 (0.7)	4.96 (1.6)	.13	NS
Cholic acid	36,969 (34,913)	26,479 (14,397)	.55	NS
Chenodeoxycholic acid	894 (576)	438 (293)	.16	NS
Ursodeoxycholic acid	6233 (6074)	6013 (11,972)	.97	NS
Hyodeoxycholic acid	3120 (1686)	4459 (2113)	.3	NS
Deoxycholic acid	225,038 (138,771)	207,850 (118,455)	.83	NS
7 $\alpha$ -Hydroxy-3-oxo-5 $\beta$ cholan-24-oic acid	60,548 (34,305)	65,314 (47,859)	.86	NS
Lithocholic acid	129,624 (75,022)	67,925 (95,275)	.28	NS
Nutriacholic acid	6973 (6269)	4733 (5455)	.56	NS
3-Oxocholeic acid	1674 (1290)	1303 (483)	.56	NS
3 $\alpha$ -6 $\beta$ -7 $\beta$ -trihydroxycholenoic acid	216,010 (167,821)	153,004 (66,865)	.46	NS
Glycodeoxycholic acid	53.6 (60.11)	30.4 (8.5)	.42	NS
Glycocholic acid	125.4 (44.8)	183.8 (64.5)	.14	NS
Taurodeoxycholic acid	2560 (2438)	893.6 (734)	.18	NS
Taurocholic acid	7526 (3499)	4973 (2591)	.23	NS

NOTE. Ten total fecal samples for analysis: the number of fecal samples per group = 5.

<sup>a</sup>P < .05 was considered significant.

using bioluminescence imaging (IVIS/Lumina; PerkinElmer, Waltham, MA).

### Eating Regimen, Alcohol, and Polyposis Experiments

TS4/APC mice<sup>28</sup> were from a B6 background and were double heterozygous for the deletion of *Apc* in the colon and terminal ileum epithelium and were used to model CRC.<sup>64,65</sup> In the initial phase (Figure 2), 4-week-old male TS4/APC mice (n = 5 per experimental group) were subjected to one of the following food and alcohol access regimens for 12 weeks: food access during the dark/active period (RTE) or light/inactive period (WTE), with access to alcohol or water. Final groups included RTE + alcohol, WTE + alcohol, vs water-treated groups of RTE + water, WTE + water, as well as water ad libitum.

Access to alcohol was provided during the feeding period, with water provided during the nonfeeding time; nonalcohol (water)-treated groups had 24-hour access to water. Alcohol was introduced at 3% and gradually increased to 15% by week 6. To mimic human conditions, animals had unrestricted access to food and liquids during the weekends.

For the time course study (Figure 4), TS4/APC mice (n = 5 per group) were subjected to the control water/H<sub>2</sub>O (RTE + water) or WTE + alcohol regimens for 6, 8, and 12 weeks.

For the prebiotic (TD160445) treatment study (Figure 5), TS4/APC mice were subjected to a WTE + alcohol regimen with standard rodent chow or with the TD160445 high-fiber diet (n = 10 per group). The prebiotic TD160445 diet was based on Envigo 2018, modified with 20% insoluble fermentable fiber by weight.<sup>28</sup>

To eliminate the immediate effects of food timing on the tissue read-outs, animals had free access to food and water 24 hours before death, which occurred at week 12 at ZT0. Body weight and average food and liquid intake were measured weekly. Two weeks before the termination of each experiment, mice were placed into empty nonbedded cages for 24 hours for microbial analysis stool collection, followed by permeability testing as described later. At termination time points, animals were killed by decapitation and their intestinal tissues were collected. Intestine was removed, opened longitudinally, and polyps were counted under a dissection microscope. Polyp diameters were measured in 2 perpendicular directions and averaged.

### Histology and Tissue Staining

Paraffin-embedded intestinal tissue was cut into 5- $\mu$ m sections, which were deparaffinized, stained with H&E, and visualized using a Leica DMR microscope (Leica Microsystems, Wetzlar, Germany). Adenomas were graded by a gastrointestinal pathologist blinded to the treatments.

For immunofluorescence analysis, after baking, deparaffinization, rehydration, and antigen retrieval in DAKO Target Retrieval Solution (S1699; Agilent Technologies, Inc, Santa Clara, CA), the slides were blocked with 3% donkey serum (017-000-121; Jackson ImmunoResearch, West Grove, CA) overnight, followed by overnight incubation with 1:200-diluted primary antibodies (FOXP3, 14-5773-82; eBioscience, San Diego, CA; CD3, 5690; Abcam, Cambridge, UK; phospho-Stat3, 9145; Cell Signaling, Danvers, MA) and a 1-hour incubation with 1:500-diluted secondary antibodies (Alexa Fluor donkey anti-rat 488, A21208, or anti-rabbit 555, A31572; Invitrogen, Eugene, OR). Sections then were

4',6-diamidino-2-phenylindole–stained and mounted using Fluoromount Aqueous Mounting Medium (F4680; Sigma-Aldrich, St. Louis, MO). ROR $\gamma$ t detection comprised the following steps: blocking with 10% horse serum for 1 hour; 1:25-diluted anti-ROR $\gamma$ t (14-6988-82; eBioscience) for 45 minutes; 1:500-diluted cross-absorbed Alexa Fluor donkey anti-rat 488 (A21208; Invitrogen) for 45 minutes; blocking with 10% rat serum (2337141; Jackson ImmunoResearch) for 1 hour; 1:200-diluted cross-absorbed tertiary Anti-Fluorescein/Oregon Green 488 (A11090; Invitrogen) for 45 minutes; 1:200-diluted cross-absorbed quaternary Alexa Fluor donkey anti-rabbit 488 (A21206; Invitrogen) antibody for 45 minutes; and 4',6-diamidino-2-phenylindole staining and mounting.

Immunoperoxidase staining was performed as previously described,<sup>28</sup> using 1:400 anti-CD4 (NBP1-19371; Novus Biologicals, Centennial, CO) and 1:500 biotinylated goat anti-rabbit (BA-1000; Vector Laboratories, Burlingame, CA). After a 75-minute incubation in ABC Complex (Vector Laboratories), diaminobenzidine (D5637-IG; Sigma-Aldrich) was used for color development in the presence of hydrogen peroxide for 6–7 minutes. The slides were counterstained with hematoxylin and bluing solution for light-field microscopy.

### Microscopic Analysis

Immunofluorescence images were acquired using an Olympus IX81 microscope (Tokyo, Japan) at 40 $\times$  magnification. Cells fluorescing both green and red were eliminated as false positives. Manual counting was performed by individuals blinded to the treatments. The surface area of the tissues was determined using BioPix (BioPix AB, Göteborg, Sweden), excluding the background and adventitia, resulting in a number of positive cells per square millimeter. Unless specified, for each immune marker in the TS4/APC polypoid mice, several tumors (average, 3–5) were imaged per mouse, with 3–5 images taken from various fields of the polyp to represent the tumor.

Immunoperoxidase images were obtained using a Leica DMR microscope at 63.3 $\times$  magnification. ImageJ software (National Institutes of Health, Bethesda, MD) was used to enhance positive cells for manual counting. BioPix was used to determine the surface area by eliminating background and obtaining the tissue per image, resulting in positive cells per square millimeter.

### Flow Cytometry

Cells from mesenteric lymph nodes were prepared and suspended in phosphate-buffered saline containing 2% fetal calf serum. A total of 2  $\times$  10<sup>6</sup> cells per 100- $\mu$ L staining volume were transferred to a 96-well V-shaped plate (lot 26218040; Corning, Kennebunk, ME), and pelleted by centrifugation for 5 minutes at 4°C at 300g. All single cells were incubated with culture supernatant from the 2.4G2 hybridoma (a gift from Dr Tom Beito, Antibody Hybridoma Core, Mayo Clinic, Rochester, MN) to block nonspecific binding of antibodies before staining for 20 minutes on ice and washed with phosphate-buffered saline. Cells then were incubated for 30 minutes on ice with antibodies against cell

surface markers. CD4-Peridinin chlorophyll protein-Cyanine5.5 (dilution: 1:300; lot: B273144; clone: RM4-5), CD8–fluorescein isothiocyanate (dilution: 1:200; lot: B217242; clone: 53-6.7), CD25-Brilliant Violet 650 (dilution: 1:200; lot: B266126; clone: PC61), and PE/Cy7 anti-human/mouse/rat CD278 (ICOS) Antibody (dilution: 1:200; lot: B213626; clone: C398.4A) were purchased from BioLegend (San Diego, CA). Dead cells were excluded using the Live/Dead Violet Dead cell Stain kit (dilution: 1:750; lot: 2008657; Invitrogen by Thermo Fisher Scientific). For intracellular staining, cells were fixed and permeabilized using a Foxp3/Transcription Factor Staining Buffer kit (lot: 1920793; eBioscience by Thermo Fisher Scientific). An intracellular antibody mixture, 100  $\mu$ L per sample, was prepared in 1 $\times$  wash/Permeabilization Buffer (cat. 00-8222, eBioscience by Thermo Fisher Scientific) and incubated for 2 hours on ice at 4°C. Intracellular antibodies included Foxp3-APC (dilution: 1:200; lot: 1936921; FJK-16s; eBioscience) and ROR $\gamma$ t-PE (dilution: 1:200; lot: 7201863; clone: Q31-378; BD Biosciences, San Jose, CA). Cells then were centrifuged and washed twice using the wash/perm buffer, and samples were transferred in a 250- $\mu$ L volume, and run on aBD LSRFortessa X20 flow cytometer (BD Biosciences). Data were analyzed using FlowJo software (Tree Star, Inc, Ashland, OR).

### Colon Permeability

In vivo colon permeability was assessed as previously described.<sup>13</sup> Briefly, mice were fasted for 8 hours before test initiation at ZT0. Solution (200  $\mu$ L) containing sucralose (0.45 mg) was gavaged, followed by subcutaneous saline injection to promote urine output. Mice were placed in metabolic cages and urine was collected for 5 hours. Permeability was calculated by measuring urinary sugar concentrations via gas chromatography and was expressed as the percentage excretion of the oral sugar dose.<sup>31</sup>

### Microbiota Profiling and Bioinformatics Analysis

DNA extraction, 16S ribosomal RNA V4 variable region amplification,<sup>66</sup> sample preparation, and modified 2-step targeted amplicon sequencing<sup>67</sup> using an Illumina MiSeq (Illumina, San Diego, CA) were performed. Sequence processing, quality assessment, clustering, and biological observation matrix analysis were performed as previously described.<sup>17,28</sup> Raw biological sequence text-based format and its corresponding quality scores (FASTQ) data were deposited in the NCBI Sequence Read Archive.

The  $\alpha$  (within-sample) and  $\beta$  (between-sample) diversity indices and ANOSIM calculations were used to examine differences in microbial community composition as previously described.<sup>28</sup> Differences in the relative abundance of individual taxa were assessed using Quantitative Insights Into Microbial Ecology (QIIME),<sup>68</sup> as previously described.<sup>28</sup>

### Fecal Metabolite Determination

Murine fecal content samples collected after treatment were processed as previously described.<sup>28</sup> Briefly, stool was homogenized in carbonate-phosphate buffer (1 part feces

with 3 parts buffer), followed by centrifugation. Internal standard (5% phosphoric acid, containing 50 mmol/L of 4-methylvaleric acid and 8% of copper sulfate) was loaded with the supernatant.

SCFA analysis was performed by gas chromatography equipped with a Nukol-fused silica capillary column (Sigma-Aldrich) and a flame ionization detector (GC-FID 7890A; Agilent), as described previously.<sup>69</sup> Total butyrate as well as the relative butyrate level (ratio of butyrate to the total SCFA level) was calculated.

Mouse stool samples were analyzed for bile acid quantification at the Proteomics and Metabolomics Facility of Colorado State University (Fort Collins, CO). Briefly, lyophilized samples were hydrolyzed in the presence of 0.1 mol/L sodium hydroxide followed by protein precipitation with acetonitrile and the addition of internal standards. Supernatant was analyzed on a Waters Acquity Ultra Performance Liquid Chromatography coupled to a Waters Xevo TQ-S triple quadrupole mass spectrometer (Milford, MA). A calibration curve was generated using authentic standards for each compound, and their corresponding stable isotope labeled internal standards in neat solution. Peak areas extracted for target compounds were normalized to the peak area of the appropriate internal standard in each sample.<sup>70</sup>

### Cell Culture and Western Blot

Caco2 cells ( $\sim 10^5$  cells) were combined with 50 pmol of small interfering RNA in 100  $\mu$ L Lipofectamine (Invitrogen) and 100  $\mu$ L Opti-MEM (Invitrogen). GPR109A small interfering RNA (sc105529) and control (sc37007) small interfering RNA were used for GPR109A knockdown. Protein extraction and Western blot were performed as previously described.<sup>28</sup> Blots were probed overnight with anti-GPR109A (1:1000, sc-377292; Santa Cruz Biotechnology, Dallas, TX), CCL28 (1:1000, LS-C379500; LifeSpan Bio-Sciences, Seattle, WA), phospho-Stat3 (1:2000, 9145; Cell Signaling Technologies), or anti- $\beta$ -actin (1:5000, A2066; Sigma-Aldrich) antibodies, followed by incubation with 1:2000-diluted horseradish-peroxidase-conjugated anti-rabbit IgG (7074S; Cell Signaling). A densitometry analysis was performed using ImageJ software.

### Statistics

Analyses of  $\alpha$  diversity indices (within-sample) and  $\beta$  diversity indices (between-sample) were used to examine changes in fecal microbial community structure within each mouse and between experimental conditions. The  $\alpha$  diversity indices (ie, Shannon, Simpson, richness, and evenness) were generated using the vegan package implemented in the R programming environment (<https://cran.r-project.org>, <https://github.com/vegandevs/vegan>). The  $\alpha$  diversity indices were calculated as follows: Shannon index ( $H' = -\sum \text{sum} [P_i/\log(P_i)]$ ), where  $P_i$  = the relative abundance of each taxon), Simpson index ( $[D = \sum(P_i^2)]$ ), where  $P_i$  = the relative abundance of each taxon), richness (number of taxa present in each sample), and Pielou's evenness ( $[J' = H'/\log(S)]$ ), where  $S$  = number of taxa present in each sample). Differences in  $\alpha$  diversity indices between groups

were assessed for significance using 1-way or 2-way ANOVA and adjusted using the FDR correction (FDR – Benjamini and Hochberg).

To examine  $\beta$  diversity differences in microbial community composition between samples, pairwise Bray–Curtis dissimilarity (nonphylogenetic) metric was generated using the Primer7 software package (Primer-E, Ltd, Quest Research Limited, Albany, Auckland, New Zealand) and used to perform ANOSIM calculations. ANOSIM was performed at the taxonomic level of genus on square-root-transformed data, and data were visualized using multidimensional scaling. To further compare microbial community structure, both within-group and between-group Bray–Curtis similarity (1 = similarity; 0 = dissimilarity) scores were generated at the taxonomic level of genus. Differences in the relative abundance of individual taxa between groups were assessed for significance using the Kruskal–Wallis test on centered log ratio transformed data, with FDR-corrected  $P$  values reported. Adjusted  $P$  values were considered significant at  $FDR < 0.05$ ; trends at  $P < .05$  also are reported. The software package Linear Discriminant Analysis Effect Size was used to identify biologically meaningful features differentiating groups, and ComplexHeatmaps in the R environment was used to depict differential feature abundances between groups.<sup>71,72</sup> Differences between groups in the summed relative abundance of putative SCFA-producing genera were tested using either the Mann–Whitney  $U$  test or the Kruskal–Wallis test. Graphs were created using GraphPad Prism (v8.00; GraphPad Software, Inc, La Jolla, San Jose, CA).

For *Per2::luc* analysis, given the established rhythmicity of *Per2* in the mouse tissue of approximate 24-hour periodicity,<sup>73</sup> a single cosinor method was used to analyze the data over time as described.<sup>74</sup>

The equation for the cosinor fit is as follows:  $Y(t) = M + A\cos(2\pi t/\tau + \phi)$ , where  $M$  is the mesor (midline statistic of rhythm, a rhythm-adjusted mean),  $A$  is the amplitude (a measure of half the extent of the variation within the cycle),  $\phi$  is the acrophase (a measure of the time of overall highest value), and  $\tau$  is the period. The fit of the model was determined by the residuals of the fitted wave.<sup>75</sup> Based on a 24-hour period, a multivariate Wald test was used to test the null hypothesis that the mesor, amplitude, or acrophase differed by the covariate (right time or wrong time feeding). Circular plots were computed on Oriana (Kovach Computing Services, Wales, UK). Statistics were performed in R (version 3.5.2) in the cosinor package.

For nonmicrobial data, numeric results were compared using an unpaired  $t$  test with GraphPad Prism 8 and are shown as means  $\pm$  SD.  $P < .05$  was considered significant.

All authors had access to the study data and had reviewed and approved the final manuscript.

### References

1. Bishehsari F, Mahdavinia M, Vacca M, Malekzadeh R, Mariani-Costantini R. Epidemiological transition of colorectal cancer in developing countries: environmental factors, molecular pathways, and opportunities for prevention. *World J Gastroenterol* 2014;20:6055–6072.

2. Arnold M, Sierra MS, Laversanne M, Soerjomataram I, Jemal A, Bray F. Global patterns and trends in colorectal cancer incidence and mortality. *Gut* 2017;66:683–691.
3. Fedirko V, Tramacere I, Bagnardi V, Rota M, Scotti L, Islami F, Negri E, Straif K, Romieu I, La Vecchia C, Boffetta P, Jenab M. Alcohol drinking and colorectal cancer risk: an overall and dose-response meta-analysis of published studies. *Ann Oncol* 2011;22:1958–1972.
4. Zhu JZ, Wang YM, Zhou QY, Zhu KF, Yu CH, Li YM. Systematic review with meta-analysis: alcohol consumption and the risk of colorectal adenoma. *Aliment Pharmacol Ther* 2014;40:325–337.
5. Aleksandrova K, Pischon T, Jenab M, Bueno-de-Mesquita HB, Fedirko V, Norat T, Romaguera D, Knuppel S, Boutron-Ruault MC, Dossus L, Dartois L, Kaaks R, Li K, Tjonneland A, Overvad K, Quiros JR, Buckland G, Sanchez MJ, Dorransoro M, Chirlaque MD, Barricarte A, Khaw KT, Wareham NJ, Bradbury KE, Trichopoulou A, Lagiou P, Trichopoulos D, Palli D, Krogh V, Tumino R, Naccarati A, Panico S, Siersema PD, Peeters PH, Ljuslinder I, Johansson I, Ericson U, Ohlsson B, Weiderpass E, Skeie G, Borch KB, Rinaldi S, Romieu I, Kong J, Gunter MJ, Ward HA, Riboli E, Boeing H. Combined impact of healthy lifestyle factors on colorectal cancer: a large European cohort study. *BMC Med* 2014;12:168.
6. Wimberly AL, Forsyth CB, Khan MW, Pemberton A, Khazaie K, Keshavarzian A. Ethanol-induced mast cell-mediated inflammation leads to increased susceptibility of intestinal tumorigenesis in the APC Delta468 min mouse model of colon cancer. *Alcohol Clin Exp Res* 2013;37(Suppl 1):E199–E208.
7. Shukla PK, Chaudhry KK, Mir H, Gangwar R, Yadav N, Manda B, Meena AS, Rao R. Chronic ethanol feeding promotes azoxymethane and dextran sulfate sodium-induced colonic tumorigenesis potentially by enhancing mucosal inflammation. *BMC Cancer* 2016;16:189.
8. Janakiram NB, Rao CV. The role of inflammation in colon cancer. *Adv Exp Med Biol* 2014;816:25–52.
9. Yehuda-Shnaidman E, Schwartz B. Mechanisms linking obesity, inflammation and altered metabolism to colon carcinogenesis. *Obes Rev* 2012;13:1083–1095.
10. Knackstedt RW, Moseley VR, Wargovich MJ. Epigenetic mechanisms underlying diet-sourced compounds in the prevention and treatment of gastrointestinal cancer. *Anticancer Agents Med Chem* 2012;12:1203–1210.
11. Demarzo MM, Martins LV, Fernandes CR, Herrero FA, Perez SE, Turatti A, Garcia SB. Exercise reduces inflammation and cell proliferation in rat colon carcinogenesis. *Med Sci Sports Exerc* 2008;40:618–621.
12. Ali T, Choe J, Awab A, Wagener TL, Orr WC. Sleep, immunity and inflammation in gastrointestinal disorders. *World J Gastroenterol* 2013;19:9231–9239.
13. Summa KC, Voigt RM, Forsyth CB, Shaikh M, Cavanaugh K, Tang Y, Vitaterna MH, Song S, Turek FW, Keshavarzian A. Disruption of the circadian clock in mice increases intestinal permeability and promotes alcohol-induced hepatic pathology and inflammation. *PLoS One* 2013;8:e67102.
14. Voigt RM, Forsyth CB, Keshavarzian A. Circadian disruption: potential implications in inflammatory and metabolic diseases associated with alcohol. *Alcohol Res* 2013;35:87–96.
15. Bishehsari F, Levi F, Turek FW, Keshavarzian A. Circadian rhythms in gastrointestinal health and diseases. *Gastroenterology* 2016;151:e1–e5.
16. Schernhammer ES, Laden F, Speizer FE, Willett WC, Hunter DJ, Kawachi I, Fuchs CS, Colditz GA. Night-shift work and risk of colorectal cancer in the nurses' health study. *J Natl Cancer Inst* 2003;95:825–828.
17. Bishehsari F, Saadalla A, Khazaie K, Engen PA, Voigt RM, Shetuni BB, Forsyth C, Shaikh M, Vitaterna MH, Turek F, Keshavarzian A. Light/dark shifting promotes alcohol-induced colon carcinogenesis: possible role of intestinal inflammatory milieu and microbiota. *Int J Mol Sci* 2016;17.
18. Stokkan KA, Yamazaki S, Tei H, Sakaki Y, Menaker M. Entrainment of the circadian clock in the liver by feeding. *Science* 2001;291:490–493.
19. Hoogerwerf WA, Hellmich HL, Cornelissen G, Halberg F, Shahinian VB, Bostwick J, Savidge TC, Cassone VM. Clock gene expression in the murine gastrointestinal tract: endogenous rhythmicity and effects of a feeding regimen. *Gastroenterology* 2007;133:1250–1260.
20. Reid KJ, Baron KG, Zee PC. Meal timing influences daily caloric intake in healthy adults. *Nutr Res* 2014;34:930–935.
21. Kahleova H, Lloren JI, Mashchak A, Hill M, Fraser GE. Meal frequency and timing are associated with changes in body mass index in Adventist Health Study 2. *J Nutr* 2017;147:1722–1728.
22. Stockman NK, Schenkel TC, Brown JN, Duncan AM. Comparison of energy and nutrient intakes among meals and snacks of adolescent males. *Prev Med* 2005;41:203–210.
23. Kant AK, Graubard BI. 40-year trends in meal and snack eating behaviors of American adults. *J Acad Nutr Diet* 2015;115:50–63.
24. Gounaris E, Blatner NR, Dennis K, Magnusson F, Gurish MF, Strom TB, Beckhove P, Gounari F, Khazaie K. T-regulatory cells shift from a protective anti-inflammatory to a cancer-promoting proinflammatory phenotype in polyposis. *Cancer Res* 2009;69:5490–5497.
25. Furusawa Y, Obata Y, Fukuda S, Endo TA, Nakato G, Takahashi D, Nakanishi Y, Uetake C, Kato K, Kato T, Takahashi M, Fukuda NN, Murakami S, Miyauchi E, Hino S, Atarashi K, Onawa S, Fujimura Y, Lockett T, Clarke JM, Topping DL, Tomita M, Hori S, Ohara O, Morita T, Koseki H, Kikuchi J, Honda K, Hase K, Ohno H. Commensal microbe-derived butyrate induces the differentiation of colonic regulatory T cells. *Nature* 2013;504:446–450.
26. Arpaia N, Campbell C, Fan X, Dikij S, van der Veeken J, deRoos P, Liu H, Cross JR, Pfeffer K, Coffey PJ, Rudensky AY. Metabolites produced by commensal bacteria promote peripheral regulatory T-cell generation. *Nature* 2013;504:451–455.



27. Pryde SE, Duncan SH, Hold GL, Stewart CS, Flint HJ. The microbiology of butyrate formation in the human colon. *FEMS Microbiol Lett* 2002;217:133–139.
28. Bishehsari F, Engen PA, Preite NZ, Tuncil YE, Naqib A, Shaikh M, Rossi M, Wilber S, Green SJ, Hamaker BR, Khazaie K, Voigt RM, Forsyth CB, Keshavarzian A. Dietary fiber treatment corrects the composition of gut microbiota, promotes SCFA production, and suppresses colon carcinogenesis. *Genes* 2018;9.
29. Terzic J, Grivennikov S, Karin E, Karin M. Inflammation and colon cancer. *Gastroenterology* 2010;138:2101–2114 e5.
30. Moossavi S, Bishehsari F. Inflammation in sporadic colorectal cancer. *Arch Iran Med* 2012;15:166–170.
31. Shaikh M, Rajan K, Forsyth CB, Voigt RM, Keshavarzian A. Simultaneous gas-chromatographic urinary measurement of sugar probes to assess intestinal permeability: use of time course analysis to optimize its use to assess regional gut permeability. *Clin Chim Acta* 2015;442:24–32.
32. Grivennikov SI, Wang K, Mucida D, Stewart CA, Schnabl B, Jauch D, Taniguchi K, Yu GY, Osterreicher CH, Hung KE, Datz C, Feng Y, Fearon ER, Oukka M, Tessarollo L, Coppola V, Yarovinsky F, Cheroutre H, Eckmann L, Trinchieri G, Karin M. Adenoma-linked barrier defects and microbial products drive IL-23/IL-17-mediated tumour growth. *Nature* 2012;491:254–258.
33. Pages F, Mlecnik B, Marliot F, Bindea G, Ou FS, Bifulco C, Lugli A, Zlobec I, Rau TT, Berger MD, Nagtegaal ID, Vink-Borger E, Hartmann A, Geppert C, Kolwelter J, Merkel S, Grutzmann R, Van den Eynde M, Jouret-Mourin A, Kartheuser A, Leonard D, Remue C, Wang JY, Bavi P, Roehrl MHA, Ohashi PS, Nguyen LT, Han S, MacGregor HL, Hafezi-Bakhtiari S, Wouters BG, Masucci GV, Andersson EK, Zavadova E, Vocka M, Spacek J, Petruzelka L, Konopasek B, Dunder P, Skalova H, Nemejcova K, Botti G, Tatangelo F, Delrio P, Ciliberto G, Maio M, Laghi L, Grizzi F, Fredriksen T, Buttard B, Angelova M, Vasaturo A, Maby P, Church SE, Angell HK, Lafontaine L, Bruni D, El Sissy C, Haicheur N, Kirilovsky A, Berger A, Lagorce C, Meyers JP, Paustian C, Feng Z, Ballesteros-Merino C, Dijkstra J, van de Water C, van Lent-van Vliet S, Knijn N, Musina AM, Scripcariu DV, Popivanova B, Xu M, Fujita T, Hazama S, Suzuki N, Nagano H, Okuno K, Torigoe T, Sato N, Furuhashi T, Takemasa I, Itoh K, Patel PS, Vora HH, Shah B, Patel JB, Rajvik KN, Pandya SJ, Shukla SN, Wang Y, Zhang G, Kawakami Y, Marincola FM, Ascierto PA, Sargent DJ, Fox BA, Galon J. International validation of the consensus Immunoscore for the classification of colon cancer: a prognostic and accuracy study. *Lancet* 2018;391:2128–2139.
34. Hanyuda A, Ogino S, Qian ZR, Nishihara R, Song M, Mima K, Inamura K, Masugi Y, Wu K, Meyerhardt JA, Chan AT, Fuchs CS, Giovannucci EL, Cao Y. Body mass index and risk of colorectal cancer according to tumor lymphocytic infiltrate. *Int J Cancer* 2016;139:854–868.
35. Flaherty DC, Lavotshkin S, Jalas JR, Torisu-Itakura H, Kirchoff DD, Sim MS, Lee DJ, Bilchik AJ. Prognostic utility of immunoprofiling in colon cancer: results from a prospective, multicenter nodal ultrastaging trial. *J Am Coll Surg* 2016;223:134–140.
36. Lavotshkin S, Jalas JR, Torisu-Itakura H, Ozao-Choy J, Lee JH, Sim MS, Stojadinovic A, Wainberg Z, Bifulco CB, Fox BA, Bilchik AJ. Immunoprofiling for prognostic assessment of colon cancer: a novel complement to ultrastaging. *J Gastrointest Surg* 2015;19:999–1006.
37. Salama P, Phillips M, Grieu F, Morris M, Zeps N, Joseph D, Platell C, Iacopetta B. Tumor-infiltrating FOXP3+ T regulatory cells show strong prognostic significance in colorectal cancer. *J Clin Oncol* 2009;27:186–192.
38. Correale P, Rotundo MS, Del Vecchio MT, Remondo C, Migali C, Ginanneschi C, Tsang KY, Licchetta A, Mannucci S, Loiacono L, Tassone P, Francini G, Tagliaferri P. Regulatory (FoxP3+) T-cell tumor infiltration is a favorable prognostic factor in advanced colon cancer patients undergoing chemo or chemo-immunotherapy. *J Immunother* 2010;33:435–441.
39. Frey DM, Droeser RA, Viehl CT, Zlobec I, Lugli A, Zingg U, Oertli D, Kettelhack C, Terracciano L, Tornillo L. High frequency of tumor-infiltrating FOXP3(+) regulatory T cells predicts improved survival in mismatch repair-proficient colorectal cancer patients. *Int J Cancer* 2010;126:2635–2643.
40. Matera L, Sandrucci S, Mussa A, Boffa C, Castellano I, Cassoni P. Low Foxp3 expression in negative sentinel lymph nodes is associated with node metastases in colorectal cancer. *Gut* 2010;59:419–420.
41. Blatner NR, Mulcahy MF, Dennis KL, Scholtens D, Bentrem DJ, Phillips JD, Ham S, Sandall BP, Khan MW, Mahvi DM, Halverson AL, Stryker SJ, Boller AM, Singal A, Sneed RK, Sarraj B, Ansari MJ, Oft M, Iwakura Y, Zhou L, Bonertz A, Beckhove P, Gounari F, Khazaie K. Expression of ROR $\gamma$  marks a pathogenic regulatory T cell subset in human colon cancer. *Sci Transl Med* 2012;4:164ra59.
42. Harrison OJ, Powrie FM. Regulatory T cells and immune tolerance in the intestine. *Cold Spring Harb Perspect Biol* 2013;5.
43. Tanoue T, Atarashi K, Honda K. Development and maintenance of intestinal regulatory T cells. *Nat Rev Immunol* 2016;16:295–309.
44. Ganapathy V, Thangaraju M, Prasad PD, Martin PM, Singh N. Transporters and receptors for short-chain fatty acids as the molecular link between colonic bacteria and the host. *Curr Opin Pharmacol* 2013;13:869–874.
45. Leonel AJ, Alvarez-Leite JI. Butyrate: implications for intestinal function. *Curr Opin Clin Nutr Metab Care* 2012;15:474–479.
46. Singh N, Gurav A, Sivaprakasam S, Brady E, Padia R, Shi H, Thangaraju M, Prasad PD, Manicassamy S, Munn DH, Lee JR, Offermanns S, Ganapathy V. Activation of Gpr109a, receptor for niacin and the commensal metabolite butyrate, suppresses colonic inflammation and carcinogenesis. *Immunity* 2014;40:128–139.
47. Thangaraju M, Cresci GA, Liu K, Ananth S, Gnanaprakasam JP, Browning DD, Mellinger JD,

- Smith SB, Digby GJ, Lambert NA, Prasad PD, Ganapathy V. GPR109A is a G-protein-coupled receptor for the bacterial fermentation product butyrate and functions as a tumor suppressor in colon. *Cancer Res* 2009;69:2826–2832.
48. Nguyen AV, Wu YY, Liu Q, Wang D, Nguyen S, Loh R, Pang J, Friedman K, Orlofsky A, Augenlicht L, Pollard JW, Lin EY. STAT3 in epithelial cells regulates inflammation and tumor progression to malignant state in colon. *Neoplasia* 2013;15:998–1008.
49. Rossi M, Mirbagheri S, Keshavarzian A, Bishehsari F. Nutraceuticals in colorectal cancer: a mechanistic approach. *Eur J Pharmacol* 2018;833:396–402.
50. Preuss F, Tang Y, Laposky AD, Arble D, Keshavarzian A, Turek FW. Adverse effects of chronic circadian desynchronization in animals in a "challenging" environment. *Am J Physiol Regul Integr Comp Physiol* 2008;295:R2034–R2040.
51. Sakaguchi S, Miyara M, Costantino CM, Hafler DA. FOXP3+ regulatory T cells in the human immune system. *Nat Rev Immunol* 2010;10:490–500.
52. De Simone V, Pallone F, Monteleone G, Stolfi C. Role of TH17 cytokines in the control of colorectal cancer. *Oncoimmunology* 2013;2:e26617.
53. Le Gouvello S, Bastuji-Garin S, Aloulou N, Mansour H, Chaumette MT, Berrehar F, Seikour A, Charachon A, Karoui M, Leroy K, Farcet JP, Sobhani I. High prevalence of Foxp3 and IL17 in MMR-proficient colorectal carcinomas. *Gut* 2008;57:772–779.
54. Park JH, Kotani T, Konno T, Setiawan J, Kitamura Y, Imada S, Usui Y, Hatano N, Shinohara M, Saito Y, Murata Y, Matozaki T. Promotion of intestinal epithelial cell turnover by commensal bacteria: role of short-chain fatty acids. *PLoS One* 2016;11:e0156334.
55. Hamer HM, Jonkers D, Venema K, Vanhoutvin S, Troost FJ, Brummer RJ. Review article: the role of butyrate on colonic function. *Aliment Pharmacol Ther* 2008;27:104–119.
56. Mutlu E, Keshavarzian A, Engen P, Forsyth CB, Sikaroodi M, Gillevet P. Intestinal dysbiosis: a possible mechanism of alcohol-induced endotoxemia and alcoholic steatohepatitis in rats. *Alcohol Clin Exp Res* 2009;33:1836–1846.
57. Engen PA, Green SJ, Voigt RM, Forsyth CB, Keshavarzian A. The gastrointestinal microbiome: alcohol effects on the composition of intestinal microbiota. *Alcohol Res* 2015;37:223–236.
58. Voigt RM, Forsyth CB, Green SJ, Mutlu E, Engen P, Vitaterna MH, Turek FW, Keshavarzian A. Circadian disorganization alters intestinal microbiota. *PLoS One* 2014;9:e97500.
59. Thaiss CA, Zeevi D, Levy M, Zilberman-Schapira G, Suez J, Tengeler AC, Abramson L, Katz MN, Korem T, Zmora N, Kuperman Y, Biton I, Gilad S, Harmelin A, Shapiro H, Halpern Z, Segal E, Elinav E. Trans-kingdom control of microbiota diurnal oscillations promotes metabolic homeostasis. *Cell* 2014;159:514–529.
60. Voigt RM, Summa KC, Forsyth CB, Green SJ, Engen P, Naqib A, Vitaterna MH, Turek FW, Keshavarzian A. The circadian clock mutation promotes intestinal dysbiosis. *Alcohol Clin Exp Res* 2016;40:335–347.
61. Rosselot AE, Hong CI, Moore SR. Rhythm and bugs: circadian clocks, gut microbiota, and enteric infections. *Curr Opin Gastroenterol* 2016;32:7–11.
62. Khazaie K, Zadeh M, Khan MW, Bere P, Gounari F, Dennis K, Blatner NR, Owen JL, Klaenhammer TR, Mohamadzadeh M. Abating colon cancer polyposis by *Lactobacillus acidophilus* deficient in lipoteichoic acid. *Proc Natl Acad Sci U S A* 2012;109:10462–10467.
63. Touitou Y, Touitou D, Reinberg A. Disruption of adolescents' circadian clock: the vicious circle of media use, exposure to light at night, sleep loss and risk behaviors. *J Physiol* 2016;110:467–479.
64. Khazaie K, Blatner NR, Khan MW, Gounari F, Gounaris E, Dennis K, Bonertz A, Tsai FN, Strouch MJ, Cheon E, Phillips JD, Beckhove P, Bentrem DJ. The significant role of mast cells in cancer. *Cancer Metastasis Rev* 2011;30:45–60.
65. Bishehsari F, Saadalla A, Khazaie K, Engen PA, Voigt RM, Shetuni BB, Forsyth CB, Shaikh MW, Vitaterna MH, Turek FW, Keshavarzian A. Light/dark shifting promotes alcohol-induced colon carcinogenesis: possible role of intestinal inflammatory milieu and microbiota. *Int J Mol Sci* 2017;17.
66. Caporaso JG, Lauber CL, Walters WA, Berg-Lyons D, Huntley J, Fierer N, Owens SM, Betley J, Fraser L, Bauer M, Gormley N, Gilbert JA, Smith G, Knight R. Ultra-high-throughput microbial community analysis on the Illumina HiSeq and MiSeq platforms. *ISME J* 2012;6:1621–1624.
67. Naqib A, Poggi S, Wang W, Hyde M, Kunstman K, Green SJ. Making and sequencing heavily multiplexed, high-throughput 16S ribosomal RNA gene amplicon libraries using a flexible, two-stage PCR protocol. *Methods Mol Biol* 2018;1783:149–169.
68. Caporaso JG, Kuczynski J, Stombaugh J, Bittinger K, Bushman FD, Costello EK, Fierer N, Pena AG, Goodrich JK, Gordon JI, Huttley GA, Kelley ST, Knights D, Koenig JE, Ley RE, Lozupone CA, McDonald D, Muegge BD, Pirrung M, Reeder J, Sevinsky JR, Turnbaugh PJ, Walters WA, Widmann J, Yatsunenko T, Zaneveld J, Knight R. QIIME allows analysis of high-throughput community sequencing data. *Nat Methods* 2010;7:335–336.
69. Tuncil YE, Nakatsu CH, Kazem AE, Arioglu-Tuncil S, Reuhs B, Martens EC, Hamaker BR. Delayed utilization of some fast-fermenting soluble dietary fibers by human gut microbiota when presented in a mixture. *J Funct Foods* 2017;32:347–357.
70. MacLean B, Tomazela DM, Shulman N, Chambers M, Finney GL, Frewen B, Kern R, Tabb DL, Liebler DC, MacCoss MJ. Skyline: an open source document editor for creating and analyzing targeted proteomics experiments. *Bioinformatics* 2010;26:966–968.
71. Segata N, Izard J, Waldron L, Gevers D, Miropolsky L, Garrett WS, Huttenhower C. Metagenomic biomarker discovery and explanation. *Genome Biol* 2011;12:R60.
72. Gu Z, Eils R, Schlesner M. Complex heatmaps reveal patterns and correlations in multidimensional genomic data. *Bioinformatics* 2016;32:2847–2849.

73. Yoo SH, Yamazaki S, Lowrey PL, Shimomura K, Ko CH, Buhr ED, Siepa SM, Hong HK, Oh WJ, Yoo OJ, Menaker M, Takahashi JS. Period 2: luciferase real-time reporting of circadian dynamics reveals persistent circadian oscillations in mouse peripheral tissues. *Proc Natl Acad Sci U S A* 2004;101:5339–5346.
74. Cornelissen G. Cosinor-based rhythmometry. *Theor Biol Med Model* 2014;11:16.
75. Sachs MC, Shoben A, Levin GP, Robinson-Cohen C, Hoofnagle AN, Swords-Jenny N, Ix JH, Budoff M, Lutsey PL, Siscovick DS, Kestenbaum B, de Boer IH. Estimating mean annual 25-hydroxyvitamin D concentrations from single measurements: the Multi-Ethnic Study of Atherosclerosis. *Am J Clin Nutr* 2013;97:1243–1251.

60612. e-mail: [Faraz\\_Bishehsari@rush.edu](mailto:Faraz_Bishehsari@rush.edu); fax: (312) 563–3945; or Khashayarsha Khazaie, PhD, DSc, Department of Immunology, Guggenheim 3-42-B, Mayo Clinic, Rochester, Minnesota 55901. e-mail: [Khazaie@mayo.edu](mailto:Khazaie@mayo.edu); fax: (507) 284–1637.

#### Acknowledgment

Ali Keshavarzian would like to thank Mr and Mrs Larry Field, Mr and Mrs Glass, Mr Keehn, and the Alvin Baum Family fund for their philanthropic funding. The authors thank Mrs Nailliw Zanini Preite for her assistance with animal studies.

#### Author contributions

FB, KK, AK conceived and designed the experiments; FB, PAE, RMV, MS, SW, AN, SJG, CF, EG, AS, AO, and BRH were involved in acquisition of data; BBS reviewed histopathology slides; FB, PAE, AN, SJG, GS analyzed the data; FB, KK and AK interpreted the data; FB drafted the manuscript; PAE, KK and AK edited the manuscript; FB, AK, KK obtained funding; all the authors approved the final draft.

#### Conflicts of interest

This author discloses the following: Ali Keshavarzian and Bruce Hamaker are a co-owner of Nutrabiotics, Inc, and BetterBiotics, LLC, which are prebiotic-focused companies. The TD160445 prebiotic used in this study is not a product of either company. The remaining authors disclose no conflicts.

#### Funding

Supported by National Institutes of Health grant AA025387 and a Rush Translational Sciences Consortium/Swim Across America Organization grant (F.B.); and by National Institutes of Health grants AA023417 and AA026801 (A.K.), and grant AA023417 (K.K.).

---

Received March 18, 2019. Accepted October 28, 2019.

#### Correspondence

Address correspondence to: Faraz Bishehsari, MD, PhD, Division of Digestive Diseases and Nutrition, Rush University Medical Center, Professional Building, 1725 West Harrison Street, Suite 207, Chicago, Illinois